Progress in Polymer Science 39 (2014) 959–978

Contents lists available at ScienceDirect

Progress in Polymer Science

journal homepage: www.elsevier.com/locate/ppolysci

Polymer extension flows and instabilities

A.Ya. Malkin[a,*], A. Arinstein[b], V.G. Kulichikhin[c]

[a] Institute of Petrochemical Synthesis, Russian Academy of Sciences, 29 Leninkii Prospect, Moscow 119991, Russia
[b] Department of Mechanical Engineering, Technion – Israel Institute of Technology, Haifa 32000, Israel
[c] M.V. Lomonosov Moscow State University, Department of Colloid Chemistry, 1/3 Leninskie Gory, Moscow 119991, Russia

ARTICLE INFO

Article history:
Received 16 July 2013
Received in revised form 14 February 2014
Accepted 17 February 2014
Available online 28 February 2014

Keywords:
Uniaxial extension
Flow-to-rubbery transition
Strain hardening
Surface instability
Filament breakup
Electrospinning

ABSTRACT

The basics of the uniaxial stretching of polymer melts and solutions are considered, including analysis of the transient regimes of deformation, as well as the different types of instability in the final stage of stretching which result in breakup of the systems in question. A steady flow can be realized only at low deformation rates. Increase in the strain rate leads to large draw ratios that can be reached only by development of elastic (reversible) deformations of a polymer, while the flow (irreversible deformations) is practically suppressed.

High rate deformations of polymer melts and solutions consisting of entangled chains are quite similar to the stretching of cured rubber. Quantitative conditions of breakup for polymer melts are also similar to the rupture of cured rubber. Thus, one can treat high rate large elastic deformations of linear polymers in stretching as strain-induced transition to the rubber-like state. This mechanism of extensional deformations is clearly seen in experiments with linear monodisperse polymers. However, similar physical processes also take place for polydisperse and branched polymers, though they are more complicated; and special phenomena such as strain hardening are observed.

In the stretching of dilute or semi-dilute solutions, surface effects begin to play an essential role. However, in this case, elasticity also stabilizes a stream, creating a highly oriented core within a filament. In dilute solutions, a solvent forms a regular structure on this core ("bead-on-a-string" structure) while in entanglement solutions, it is squeezed out of a filament, forming separate drops. The latter is reminiscent of the stress-induced phase separation effect. Concentration redistribution along and across a filament then occurs, leading to modification of its temporal and spatial rheological properties.

A special case of strong (high strain rate) stretching of polymer solutions is electrospinning, which is accompanied by loss of solvent.

In all cases of high rate stretching, elastic deformations inherently related to macromolecules are dominant.

Contents

* Corresponding author.
E-mail address: alex_malkin@mail.ru (A.Ya. Malkin).

http://dx.doi.org/10.1016/j.progpolymsci.2014.02.006
0079-6700/

1. Introduction

Extensional flows of polymer solutions and melts and their stability are of great interest for fundamental science as well as for technology. There are a great variety of situations in which such flows are important. Very well known examples are in fire fighting and engine technology, as well as ink-jet printing and medical diagnostics, cosmetics and agricultural irrigation. Stability of extensional flow is directly related to the fundamental aspects of physics, applied mechanics and computational mathematics. The stability and breakup of polymeric filaments are controlled by properties of macromolecules: by their length, rigidity, intermolecular interactions and solubility in a solvent, by the rheology of a fluid, etc.

The issue of breakup of the polymeric filament in extension is a permanent challenge for both academic interest and applications. Though the first classical survey [1] and a study of stream instability in the linear approximation [2] were published in the middle of the nineteenth century, new studies devoted to this phenomenon are continually appearing in periodicals (see a review [3] for a comprehensive historical essay on the problem). The competition of surface forces and viscosity is a driving force for instability ("capillary instability") of numerous low molecular-weight liquids.

The introduction of polymers, either as a solution or melt, into this field created a new situation and a vast array of problems for research. The basic issue in discussing polymer solutions is the peculiarity of their behavior in terms of the elasticity of these fluids. This is not essential in slow flows but becomes a dominant factor in so called "strong flows." The latter can be defined as regimes of deformation in which the deformation rate becomes much higher than the reciprocal relaxation time or the Weissenberg Number, *Wi*, is much higher than (1). In this case, we have to consider a filament not as a liquid but rather as a rubbery (elastic) fiber. The dynamic transition from a fluid to a rubbery state determines many peculiarities of the observed effects in strong flows of polymer solutions and melts in uniaxial extension (by the way, this resembles shearing). It is worth recalling that instability in shear flows of polymeric and micellar colloid fluids is also determined mainly by their elasticity [4,5].

This review is organized in the following manner. First, we briefly discuss the experimental principles used for studying uniaxial extension (see Section 2). Thereafter, we focus on the experimental results obtained in examining the main peculiarities controlling extension in different deformation regimes (see Section 3). In this section, homogeneous extension that finishes with the breakup of a filament (that is typical for the melts of monodisperse linear polymers), as well as the strain hardening effect observed for polymer melts with macromolecules of more complicated architecture, are systematically considered. Next, we discuss the extension mechanism of polymer solutions resulting in the formation of a regular structure along a filament, and, perhaps, a phase separation. The final part of Section 3 is devoted to the rather special extension type occurring in polymer solutions during electrospinning, utilized for nano-fiber fabrication. Finally, in Section 4, the main physical aspects of the polymer extension are discussed.

2. Experimental methods

There are several experimental schemes for measuring the rheology of uniaxial extension [6]. Below, we discuss only substances that can flow (at least, being initially fluid, though they can transform to solid-like filaments in the process of extension).

The most evident one is stretching a preformed cylindrical sample with fixed ends. The sample is drawn by one (or both) ends with either constant or programmed velocity or force. In the first approximation, it is assumed that the stretching proceeds homogeneously along the length of the sample. In this case, it is easy to calculate stresses and deformation rates and to consider these data in frames of this or that rheological model.

The basic assumption in extension experiments is the homogeneity of deformations and this point should be always accurately followed in either stress- or rate-controlled testing. If a sample is extended homogeneously with velocity $v(t)$, the length l of the sample increases according to the following equation

$$l(t) = l_0 + \int_0^t v(t)dt \tag{1}$$

where l_0 is the initial length of a sample.

If an experimenter wants to maintain constant rate of deformation $\dot{\varepsilon}$ the velocity should increase according to the following equation

$$v(t) = \dot{\varepsilon} l_0 \exp(\dot{\varepsilon} t) \tag{2}$$

Usually, it is assumed that the volume of a sample does not change in extension. Therefore it is easy to find the area of the sample's cross-section knowing the length of

the sample and to calculate the normal stress at any time of extension.

An option in this experimental scheme is to cut a sample after extension and observe its elastic recoil. It is worth mentioning that this method of separation of the full deformation into irreversible deformations (flow) and elastic parts is rigorous enough only in the linear viscoelastic behavior range. Besides, if elastic recoil continues for too long, the surface tension becomes dominant, and the sample transforms into a ball; this has nothing in common with elastic deformation.

The second experimental method consists in the flow of a free stream. In this case, a fluid is extruded from an orifice, and then moves due to inertial and gravitational forces, or a strand is taken onto a roll and drawn by rotation. The latter scheme can be realized only for a viscoelastic fluid.

The third experimental approach (called "the filament stretching rheometer") consists in the following protocol. A small quantity of liquid is placed between two plates. The plates are moved apart and the droplet transforms to a ligament. Extension of a droplet can be realized by either a free-fall extensional device [7,8] or by moving a lower plate with mechanical or electro-mechanical drive. The distance between plates can be fixed and an experimenter observes changes in the profile of the sample in time up to the break of the liquid bridge due to capillary forces. The time-dependent behavior of the filament radius and profile was followed by different optical techniques. This method was proposed in [9,10] and then developed and used for different purposes in [11–20]. One can find an exhaustive review of the earlier works that used this method in [21]. Interest in exploring this method continues to exist [22–27] and we will apply the results of those studies below in discussing the physics of the stretching and breakup of dilute solutions.

The fourth experimental technique is called the "Sentmanat Extensional Rheometer" (SER) [28,29]. It consists of two rollers having parallel axes and rotating in opposite directions. The ends of a film sample are fixed on the rollers and the sample is stretched due to the rotation of the rollers.

It is possible to find other experimental schemes; extensional flow in the conical transition from large cylinder to a small one, flow in contractions inside a cylinder, flow in the open siphon and so on. However they have not been widely used. Also, we do not discuss experimental schemes oriented to the study of individual macromolecule extension (four roll method, double jet apparatus) because the aims of such investigations are beyond the goals of this review.

3. Results

3.1. Homogeneous extension of polymer melts

A general physical understanding of the mechanism of large deformations in uniaxial extension is based on the experimental results of studies of monodisperse polymer melt behavior at constant deformation rates varying in a wide range [29–34]. Fig. 1 demonstrates the dependence of the limiting Hencky strain ε^* versus the deformation rate and the separation of this strain into viscous and elastic (rubbery) components. At a very low deformation rate (left part of the figure), elongation can be rather high. This is a domain of dominant viscous flow which is limited by capillary instability only. The most interesting is the central part between two vertical dotted lines. In this domain, rubbery deformation increases along with increasing deformation rates and finally becomes practically entire part of strain while the viscous flow appears negligible.

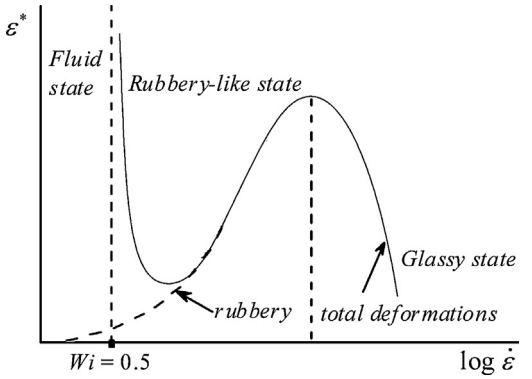

Fig. 1. Diagram ("*master curve*") of limiting deformations as a function of the deformation rate.

Fig. 1 represents the stretching of a rubber strip and the limiting strain corresponds to the strength of this strip. Therefore, this intermediate domain presents the deformation induced flow-to-rubbery transition zone and it reflects the rubber-like behavior of a melt. The right part of the diagram is a continuous transition to glassy-like behavior at very high deformation rates. The complete diagram ("master curve") can be experimentally obtained using the principle of time-temperature superposition because the range of deformation rates covers many orders of magnitude. The same understanding of the breaking length was proposed also in [35] for experiments carried out in inhomogeneous stretching.

The complete similarity in elasticity of linear and cured polymers of the same chemical nature is demonstrated in Fig. 2. The curves in Fig. 2 are quite similar and the difference in the position is explained by natural dependence of elastic modules on the network (both chemical and physical) density.

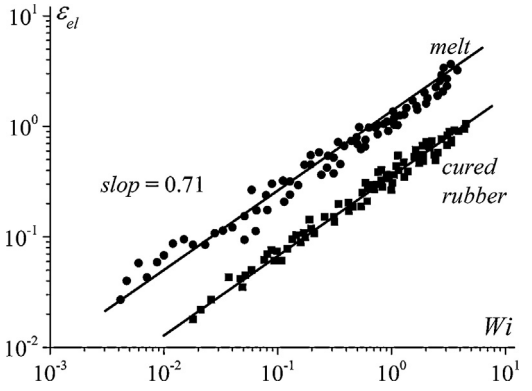

Fig. 2. Elastic properties of polyisoprene linear polymer and curved rubber for linear polymer: $\tilde{M}_w = 5.75 \times 10^5$; $\tilde{M}_w/\tilde{M}_m = 1.05$ [36,37].

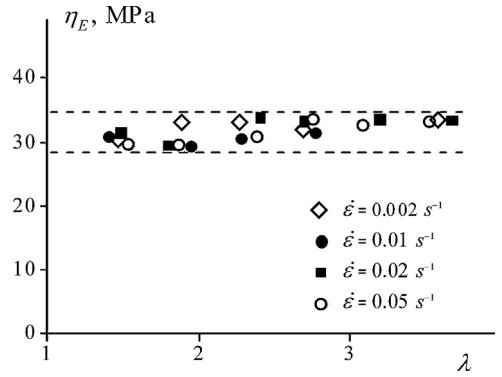

Fig. 3. Independence of the elongation viscosity, η_E, on draw ratio, λ, at different deformation rates. Polyisoprene: $\bar{M}_w = 5.75 \times 10^5$; $\bar{M}_w/\bar{M}_m = 1.05$. $T = 25\,^{\circ}C$ [31].

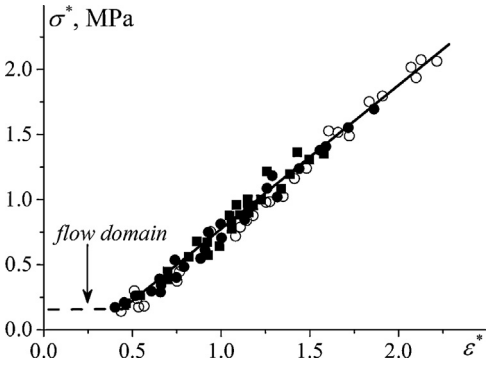

Fig. 4. Limiting strength, σ_E^* – strain, ε^*, dependence at failure for monodisperse polyisoprenes (light symbols) and polybutadienes (dark symbols). Different types of symbols correspond to different MM (for details, see [30–32]).

The possibility of a high degree of extension and stability of long polymer melt filaments are intuitively and traditionally explained by the increase in the elongational viscosity with the increase in strain. Meanwhile, direct experiments showed that, at least in monodisperse polymer melts, the apparent elongational viscosity (understood as the ratio of normal stresses to viscous deformation rate, i.e., as the measure of dissipative losses), remains practically constant up to rather high deformation rates and draw ratios [31]. This is illustrated in Fig. 3 where the elongation viscosity η_E was calculated as

$$\eta_E = \frac{\sigma}{\dot{\varepsilon}_f}, \tag{3}$$

where $\dot{\varepsilon}_f$ is the rate of irreversible (but not complete) deformation.

The stability of a jet in extension should thus be explained by the flow-to-rubber-like transition as a function of the rate of strain. The growth of transient normal stress is explained not by the growth of the elongation viscosity but by the rubbery-like deformation of filaments and growth of the elastic stresses.

If we exclude the left part of the viscous elongational flow, the diagram of limiting deformations of a melt appears quite similar to Smith's failure envelopes for cured rubbers [38]. This is not coincidental, but the consequence of the rubber-like behavior of entangled melts at high enough deformation rates. Limiting states at failure of various linear polymers are shown in Fig. 4. Actually, these data illustrates the rate dependence of the elastomer strength that is well known for cured rubbers and is also observed for melts. Breakup of stretching samples is due to overcoming cohesive forces.

It is interesting to specify the initial point of the straight line in Figure 4. It is seen that the elastic rupture becomes possible at $\varepsilon^* > 0.5$, and evidently that this limit is the critical value of the Weissenberg Number $Wi = 0.5$ corresponding to the flow-to-rubbery transition in Fig. 1 [34]. A similar approach to rupture of entangled polymers was proposed in [39,40] based on the concept of critical recoverable strain and scaling arguments.

The relaxation mechanism of rupture of fibers under normal stress is also confirmed by the effect of long-term durability under constant stress (Fig. 5). Breakup time t^* scales with the stress as a power law: σ_E^{-n}, where $n = 3$. It is interesting to note that the durability of cured rubbers is also described by the power law though with higher values of the exponent, and this exponent value approaches 3 for mild (slightly cured) rubbers. Similar data on long-term durability of polymer melts can be found in [41] though the slope of t^* versus stress dependence appears different for two different polymers.

Then it is possible to find the durability of non-cured polymers in extension, not at $\sigma = \text{const}$ but at different stress histories. It is reached by using the standard rule of superposition of damages (the so-called Bailey integral or "linear summation of damages" [42]):

$$\int_0^{t^{**}} \frac{dt}{t^*[\sigma_E(t)]} = 1, \tag{4}$$

where t^{**} is duration in any complex regime of loading and $t^*(\sigma_E)$ is the dependence obtained at $\sigma_E = \text{const}$, as in Fig. 5.

A set of different experimental facts thus confirms that homogeneous extension of polymer melts at high deformation rates occurs in a manner quite analogous to the stretching of rubber.

Now let us compare the behavior of monodisperse polymers at low and high deformation rates in extension and

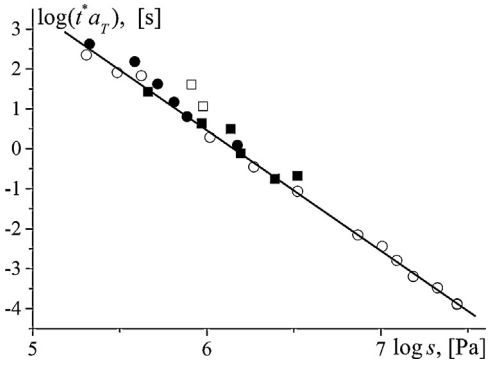

Fig. 5. Long-term strength of polymer melts under application of constant stress polybutadienes. Different symbols correspond to different temperatures in the range of −10 to 50 °C (for details, see [30–32]).

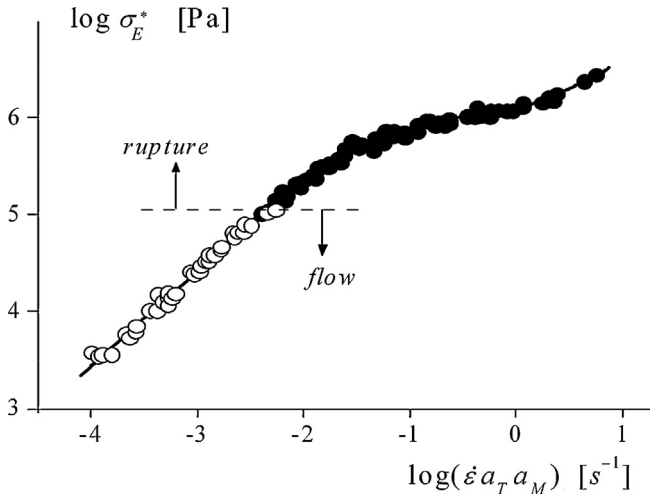

Fig. 6. Limiting states (steady flow – light symbols, rupture – dark symbols) in extension of monodisperse polybutadienes, reduced by temperature and molecular weight (*a*) and shear (*b*). a_T and a_M are shift factors for temperature and molecular weights calculated by temperature and molecular weight dependencies of the Newtonian viscosity, respectively. Temperature range of −10 to 50 °C and MM range of 3.75×10^5 to 1.7×10^6 were used in experiment (for details, see [30,31]).

shear. Fig. 6 presents the dependence of the limiting normal stress σ_E^* on the temperature and molecular weight reduced strain rate for extension. The σ_E^* values have two different meanings. Below the dashed line, σ_E^* corresponds to the steady flow and thus the light points in Fig. 6 are presenting a flow curve that can be achieved at low strain rates. Above the dashed line, a regime of the steady flow cannot be achieved, and σ_E^* are stresses corresponding to the filament breakup. Quite a similar picture is presented at Fig. 7 for shearing. Steady flow (with Newtonian viscosity) takes place at low shear rate, while at some critical shear stress σ^* the flow becomes impossible, and the melt transition from a fluid to a stress-induced rubbery state occurs.

There are several important similar features in shear and extension. It is seen that, in both cases, flow occurs only up until a certain critical stress, and above this stress flow becomes impossible. In extension, further increase of stress (or deformation rate) leads to rupture – the transition from open to dark symbols. In shear, attempting to increase the stress results in "spurt" – transition from flow to wall slip

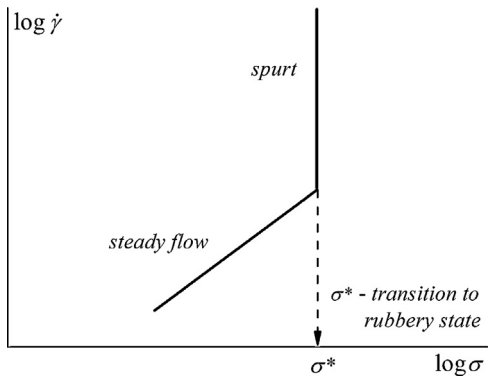

Fig. 7. Transition from flow to spurt in shearing at the critical stress σ^* (according to [43,44]).

[43,44]. Both phenomena are the consequence of a forced flow-to-rubbery transition.

We suppose that this transition happening at the critical Weissenberg Number value is related to the impossibility of slipping of macromolecules through entanglement knots and it results in the suppression of their disentanglement, due to the fact that the reciprocal deformation rate becomes shorter than the life-time (relaxation time) of a knot. Flow in the initial part of the diagram in Fig. 1 happens due to the chain mutual sliding through the entanglement knots. This process is sometimes called "yielding" [45] though this term might be deceptive. To the contrary, in the case of sufficiently high deformation rates, a tightening of the knots and a thickening of entanglement zones takes place, as was demonstrated in model experiments [37,46]. The transition of a polymer melt/solution into a rubbery state at high strains (or at sufficiently high deformation rates) is related to the locking up of chains in the entanglement knots.

Meanwhile, quite a different mechanism of high deformations with further increase in the Weissenberg Number was described and investigated in [47]. This is "shear yielding to necking", characterized by a special type of instability consisting in the sharp transition from the initial wide section of a sample into a thin sample, while further stretching is occurring as the transition from the initial section to the neck. This type of instability is very well known for solid amorphous and crystalline polymers, as well as for various metals and alloys. The transition is well defined due to visible inhomogeneous deformation. It turned out that the transition to a new type of deformation occurs at a critical stress being equal to the doubled elastic plateau modulus [48]. Coming back to the general master curve in Fig. 1, the necking mechanism is related to the increasing branch of the dependence ε^* versus log(*Wi*), when the strain is almost totally elastic (rubbery) and the flow is suppressed. So, it was shown that failure in the decreasing part of the master curve (typical rubber behavior) fundamentally differs

from the behavior corresponding to the ascending branch of the master curve, where strain localization resulting in unstable necking, occurs [47]. It means that quite different failure modes in extension can exist: capillary instability (as in fluid zone at $Wi < 0.5$ in Fig. 1), tensile decohesion, necking and rupture at very high strain rates.

It is worth emphasizing that steady regime of flow is possible only in the terminal zone ("fluid state" in the master curve of Fig. 1 at $Wi < 0.5$) [30,44]. Meanwhile, some theoretical considerations predict (according to the commonly accepted "tube model") that steady elongation flow could be realized in the wide range of Weissenberg Numbers, noticeably exceeding this limit (at least, up to $Wi = 50$); and the dependence of limiting stress is scaled with Wi by a power law with exponent equal to 0.5 [49]. However, according to the Trouton law, in the terminal zone the exponent definitely should be equal to 1.

The general meaning of the experimental results cited above may be embodied in the following conclusions:

1. Uniaxial homogeneous extension of linear monodisperse polymer melts made it possible to clear up the basic physical mechanisms of their rheology: deformation-induced transition from fluid to rubber-like behavior, absolute dominations of elastic (reversible) strains over plastic flow and just this provides a possibility of large draw ratios, impossibility of steady extension flow at high Weissenberg Numbers, rubber-like breakup and durability similar to that observed for cured rubbers.
2. A filament in extension is stabilized by its elasticity and surface effects do not play any significant role.

These experimental results and physical conclusions are the benchmark for discussing the behavior of polydisperse polymers and macromolecules with complicated molecular structure (branching and so on) because these factors superpose additional complications in the rheology of melts, that should be understood based on fundamental regularities of polymer physics.

3.2. Strain hardening

Dominant characteristics of monodisperse polymer melts were mainly discussed in Section 3.1. It is of high importance because only monodisperse samples allow us to obtain unambiguous and more definite physical results. Polydisperse polymers are mixtures of substances with different properties; and when we measure their characteristics, we obtain averaged parameters, as well as new effects, that will display different behavior and interaction of various components.

Meanwhile, studies of the extensional rheology of polydisperse polymers are interesting from two points of view. First, these materials demonstrate strong non-linear behavior and this is an experimental basis for development, testing, and application of different non-linear models of viscoelastic behavior [50–52]. Second, comparison of elongational behavior of industrial grades of polymers can be a powerful technological method for characterization

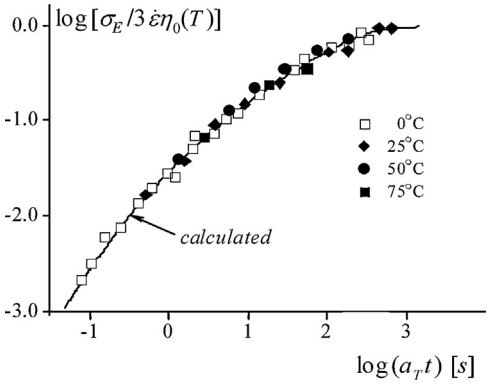

Fig. 8. Transient behavior of a polubutadiene sample at $\dot{\varepsilon} = \text{const}$. $\bar{M}_w = 1.7 \times 10^6$. Curve is calculated by Eq. (5), the points are experimental data [31,32].

and optimization of polymer structure and composition [53–55].

As shown above, two limiting types of behavior for monodisperse polymers are possible: at low Wi they come to the steady flow, whereas at high Wi the breakup (rupture) occurs.

More general and complex representation of the polymer melt rheology can be observed in measuring transient behavior in extension. Monodisperse polymer melts remain in the linear viscoelastic behavior domain for a rather wide strain rate. So, one can expect that their transient stress dependence at rate-controlled regime of deformation (at constant deformation rate) should be described by the following equation at sufficiently low deformation rates:

$$\eta_E^+ = \frac{\sigma_E}{\dot{\varepsilon}} = 3\int_{-\infty}^{\infty} \tau H(\ln\tau)[1 - \exp(-t/\tau)]\int_{-\infty}^{\infty} d\ln\tau, \qquad (5)$$

where $H(\ln\tau)$ is the relaxation spectrum.

It is easy to see that in the limit $t \to \infty$, the integral in the right-hand member of Eq. (5) gives the initial (linear) Newtonian viscosity η_0; and Eq. (5) transforms into the Trouton equation:

$$\sigma_E = 3\eta_0\dot{\varepsilon} = \eta_E\dot{\varepsilon} \qquad (6)$$

The transient behavior of a monodisperse sample, observed in the rate-controlled experiments ($\dot{\varepsilon} = \text{const}$), is depictured in Fig. 8. In order to normalize the data related to different temperatures, the above transient behavior is presented as the function $\sigma/3\dot{\varepsilon}\eta_0(T)$ versus $a_T t$ in the double-log scale. So, temperature reduction to 25 °C along stress and time axes was made by the shear Newtonian viscosity values η_0.

One can see in Fig. 8 that the dependence, calculated with the help of Eq. (5), coincides with the experimental points; and this fact demonstrates that the transient behavior of this polymer obeys the linear viscoelasticity relationships.

The situation with polydisperse and/or branched polymers appears to be much more complicated. Typical results are presented in Fig. 9. Here the transient values of the apparent viscosity η_E^+ are designated as $\eta_E^+(t) = \sigma_E^+(t)/\dot{\varepsilon}$ which should not be obligatory "viscosity" (as a measure

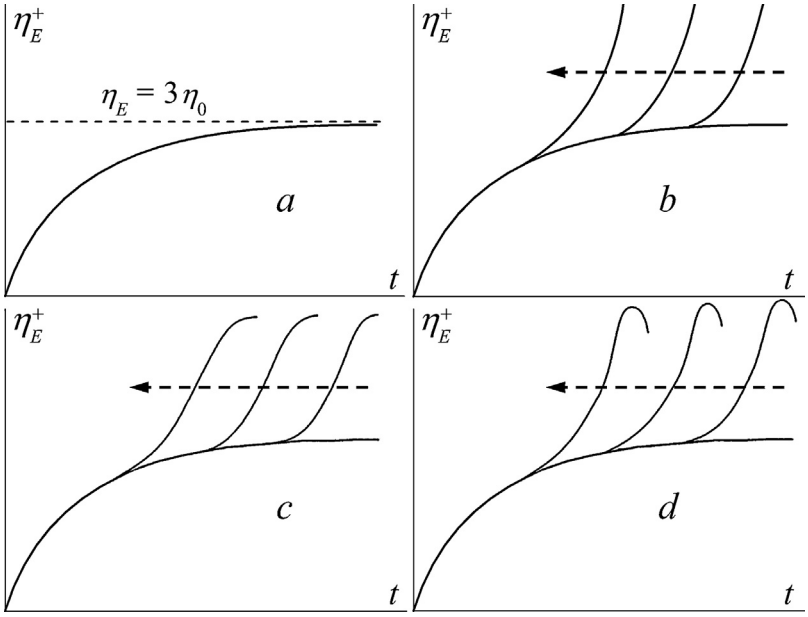

Fig. 9. Schemes illustrating development of the tensile growth stress coefficient in time: achieving steady state viscosity (*a*), and different types of strain hardening (b–d). Arrows show the direction of increasing strain rates.

of the rate of dissipation), it is simply a normalized stress σ_E^+.

One can see that steady state elongation viscosity is being achieved, and then the flow continues, until a sample breaks for one or another reason (Fig. 9a). As emphasized above, this type of time dependence is typical for extension of monodisperse polymers because their behavior at low *Wi* is determined by the linear viscoelasticity behavior [30,31]. However, the same type of behavior can also be observed in the extension of some linear polydisperse polymers [56].

Quite different types of behavior of extension, the so-called "strain hardening" effect, are shown in Fig. 9b–d. These include stress growth ending with breakup of a sample (Fig. 9b), growth for which a second plateau is observed (Fig. 9c), and behavior with a maxima (overshoot) in the tensile growth coefficient (Fig. 9d). What was perhaps the first demonstration of overshoot in a controlled regime of polystyrene extension above its glass temperature was published in [57]. However, later it was shown that this effect, observed for poly(butyl methacrylate), disappears after aging of samples [58]. It is difficult to say whether this result is common for different polymers, but undoubtedly the prehistory of a sample puts its mark on the results of further experiments.

Experimental data demonstrating strong overshoot in η_E^+ versus strain curves were also described in [59], while the apparent viscosity (tensile growth stress coefficient) after the overshoot can reach a plateau (though this plateau is almost indistinguishable if the time scale is used instead of strain). However, one can doubt the physical meaning of measurements beyond the maxima. It is believed that the existence of a maximum in the stress versus strain curve is the reflection of instability and transition from homogeneous stretching to necking [60], similar to what is well known for many solid materials. This concept is quantitatively related to the Considère criterion [61]. Application of this approach to the polymer melt stretching was recently discussed [62]. Possibly, this phenomenon is the evidence of solid-like behavior as the results of a fluid-to-non-fluid state, as was discussed for monodisperse polymers. Such a perception of breakup in a viscoelastic-to-elastic transition was confirmed using the Considère criterion in [63]. Necking with extension instability was also observed and some explanations describing apparent elongational viscosity overshoot were proposed in [64]. The nature of overshoot in extension was also discussed in [65]. However, it was thought that the problems related to this kind of instability could be avoided by performing stretching in the stress-controlled mode [62,66].

Meanwhile, it is worth mentioning that the problem of plateau and/or overshoot continues to be the subject of active discussion in the literature. For example, a clearly pronounced domain of constant viscosity at strains after a stress maximum was identified as the extensional viscosity at the given stretch rates [67]. Moreover, the viscosity values found in the constant stress and constant strain rates modes of extension coincide. They also argue that "the maximum marks a transition to a flow state in which branched polymers [with which they experimented] behave as linear polymers," and does not touch on the problem of instability and/or necking.

In the many cases the effect of "strain hardening" is definitely related to the branching of macromolecules [50,68–76]. In the general case, the effect is explained by one or another specific feature of macromolecule architecture [77,78]; and, indeed, in many cases strain hardening was experimentally observed in the melts of branched polymers. However, it is necessary to underline that the strain hardening effect is also observed in polymer

mixtures and linear polymers, prepared from fractions with different molecular weights [79–83].

It was argued in [84] that the strain hardening arises from peculiarities of the extension kinetics, and is related to the disentanglement process. Moreover, it was supposed that strain hardening can occur in any polymer, if the deformation rate is sufficient high because in that case the entanglement network can be effectively strengthened during extension.

Modeling of the extension process in the non-linear regime has been carried out mainly on the base of the Wagner model, taking into account also the influence of deformation rate on the relaxation properties of a polymer melt [51,52,82,85,86]. This type of modeling successfully described the complete deformation curves in extension. So, in the language of viscoelasticity, this approach is based on stress (or strain) induced transformation of a relaxation spectrum. It is reasonable then to suppose that, generally speaking, the difference in behavior between mono- and polydisperse polymers in extension and in shear have the similar reasons [87]. In shearing, the non-linear phenomena at high deformation rates are caused by a partial relaxation of long molecules when they are moving in the surroundings of low-molecular-weight chains. In extension, high-molecular-weight fractions can extend in a low-molecular-weight matrix, providing the increase in resistance to the given deformation rate. In both cases the non-linearity in mixtures is related to the disentanglement/tightening process, as was modeled in [36,37,88].

3.3. Treating experimental data in extension of a droplet. Instability in extension of polymer solutions: the "bead-on-a-string" structure formation

Now let us consider what new effects appear at the transition from a highly viscous elastic melt to polymer solutions. The extreme case is viscoelastic dilute and then semi-dilute entangled polymer solutions. The most widely explored experimental scheme in the study of these objects (the extension of a single filament) was discussed in Section 2 where the principal publications in this field have been cited.

The spatiotemporal evolution of a viscoelastic filament is determined by the balance of the viscosity, elasticity, gravitation, and surface tension [89]. Accordingly, the following dimensionless criteria may be constructed [27,90,91]:

1. Weber Number, $We = \rho V^2 r_0/\gamma$, the ratio of the inertia and surface tension forces (the Weissenberg Number can be defined also as $Wi = \dot{\varepsilon}\tau$);
2. Froude Number, $Fr = (V^2/gr_0)^{1/2}$, the ratio of the inertia and the gravity forces;
3. Reynolds Number, $Re = \rho V r_0/\eta$, the ratio of the inertia and the viscous forces;
4. Capillary Number, $Ca = \eta\dot{\varepsilon}/(\gamma/r_0)$, the ratio of the viscous and the surface tension forces;
5. Ohnesorge Number, $Oh = \eta/\rho\gamma r_0$ [92], which can be also expressed as $Oh = \sqrt{We}/Re$, the ratio of the viscous and the surface tension forces, analogous to the Capillary Number, Ca;
6. Deborah Number, $De = \tau/\sqrt{\rho r_0^3/\gamma}$, the final rather important dimensionless number appearing in the discussions of elastic fluids behavior.

In addition, the following dimensionless number was introduced in [93]: $El = \gamma/Er_0$, ratio of the surface forces and the elasticity forces. This new criterion may be also expressed as: $El = De/Oh$ taking into account that $E = \eta_E/\tau$.

The symbols in these formulas have the following meaning: ρ is the fluid density, η is the shear viscosity, η_E is the extensional viscosity, γ is the surface tension, r_0 is the initial radius of the filament, V is the characteristic velocity and $\dot{\varepsilon}$ is the deformation rate. In additon, τ and E are the characteristic relaxation time and the elastic modulus, respectively, associated with the polymer solution.

The theoretical analysis of filament stretching and breakup is usually considered on the base of constitutive equations starting from the Newtonian behavior and then extended to some non-linear equations of elastic fluids.

The visualization of a stream and examination its inherent structure published in some recent studies make an additional contribution to the understanding of processes occurring in viscoelastic breakup of a filament [94–96].

The problem of breakup was considered in [97–99] for Newtonian fluids. It was shown that, depending on the Ohnesorge Number and the initial filament scale, a thin filament of liquid separates into two or more droplets, or eventually is condensed lengthwise, forming a single larger droplet [98]. Indeed, surface tension governs two competing processes: namely, breakup and the tendency to the decrease of surface; and the relative time scales of both being controlled by the balance between capillary and viscous forces, determine the final result [100]. These results generalize the classical Rayleigh–Taylor analysis of the Newtonian fluid jet breakup. In any case, elasticity created by the presence of polymer molecules in a solution results in fundamentally new behavior.

As shown in Sections 3.1 and 3.2, extension of polymer melts at high deformation rates occurs in a homogeneous manner with no disturbances of any type; and the sole instability effect is rupture of a fiber. This is quite similar to extension of a cured rubber strip, which also may be stretched without any instability up to failure at some high extension ratio.

However the situation changes on passing from a melt to a relatively low-viscosity solution. Repeatedly the instability of elastic fluids which looks like the formation of a "*beads-on-a-string*" structure, consisting of drops interconnected by thin and stable filaments, has been described [101–106,90]. A very impressive example of such a structure is shown in Fig. 10, a popular image that has been reproduced in several publications. The *beads-on-a-string* filament structure is generally understood as "spherical fluid droplets are interconnected by long thin fluid ligaments" [22]. Usually, this type of instability is described for dilute polymer solutions. At the same time this phenomenon is also observed for any elastic fluids containing worm-like micelles, so these fluids are similar to polymer solutions in different aspects [107].

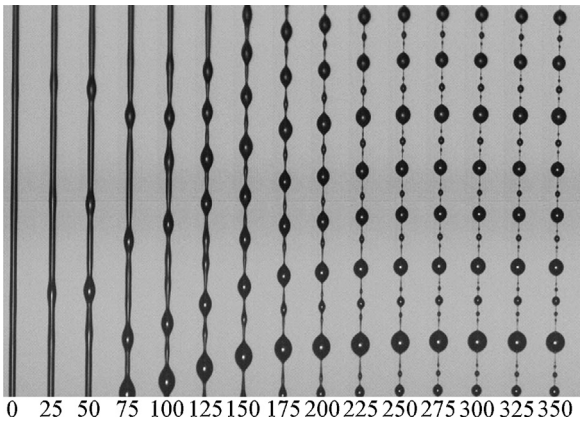

Fig. 10. Development of a "beads-on-a-string" structure. An aqueous polyethylene oxide solutions. Concentration is 0.2%. Figures below images are time in ms [104], Copyright 2005. Reproduced with permission from AIP Publishing LLC.

The origin of a bamboo-like or varicose viscoelastic filament can be considered as surface-tension-driven waves analogous to those in any viscous fluid. However, these viscoelastic filaments do not break up into separate drops (as opposed to a viscous liquid). The polymer inside the drops remains relaxed, whereas polymer macromolecules in connected cylindrical parts of the filaments between drops become strongly oriented, leading to the high strength of these bridges. The orientation of macromolecules is an obvious and experimentally confirmed consequence of liquid filament stretching [96,108,109]. This evolution of physical microstructure leads to strain hardening of a sample [110–112]. The difference in the structure of initial and highly stretched solution is also clearly seen in measuring the relaxation rate after deformation: strong deviation from a steady state leads to noticeable difference in the relaxation rates after shear and after extension, because extension results in much higher orientation than shear [100].

Theoretical understanding of instability of the viscoelastic fluid filament is based on the analyses of different constitutive models of such fluids. Usually, the following models are used for analysis: the *linear Oldroid-B model* of viscoelastic fluid [22,89,112,113], the so-called "*Finite Extensible Nonlinear Elastic*" (*FENE*) model [27,113,114], and the *Giesekus non-linear model* [114,115].

The Oldroyd-B model is formulated in the following form

$$\boldsymbol{\sigma}_p + \tau\left[\frac{\partial \boldsymbol{\sigma}_p}{\partial t} + v\cdot\nabla\boldsymbol{\sigma}_p - (\nabla v)^T\cdot\boldsymbol{\sigma}_p - \boldsymbol{\sigma}_p v\right] = 2\eta_p\mathbf{D}, \quad (7)$$

where the stress tensor $\boldsymbol{\sigma}$ is considered as the sum of two components $\boldsymbol{\sigma}_s$ and $\boldsymbol{\sigma}_p$ corresponding to the solvent and polymer contributions, respectively: $\boldsymbol{\sigma} = \boldsymbol{\sigma}_s + \boldsymbol{\sigma}_p$; the solvent flow is expressed by Newton's law: $\boldsymbol{\sigma}_s = 2\eta_s\mathbf{D}$, where $\mathbf{D}$ is the rate-of-strain tensor. There are thus three material constants; a relaxation time τ, the solvent viscosity η_s and the viscosity of the polymer η_p defined in Eq. (7).

Initially the Oldroyd-B model was proposed for an elastic dumbbell with a single relaxation time, τ; however, it can be easily generalized for a sum of relaxation modes [15]. For the single-relaxation-mode model, rheological constants of a fluid can be calculated by direct measuring the decay in the filament radius, $R(t)$, which decreases exponentially [15]:

$$\frac{R(t)}{R_p} = \left(\frac{\eta_p R_p}{\tau\sigma}\right)^{1/3}\exp\left(-\frac{t}{3\tau}\right), \quad (8)$$

where R_p is the plate radius (initial radius of a filament), η_p is the polymer solution viscosity, τ is the relaxation time, and σ is the surface tension. This equation allows one to find the relaxation time of a viscoelastic fluid if Eq. (8) is applicable.

As seen above, the Oldroyd model describes the linear-viscosity fluid. Details of the Oldroid-B fluid extension were thoroughly analyzed numerically in [109]. Taking into account the effects of viscoelasticity and inertia of a fluid, as well as the surface tension and deformability of free surface, allowed the authors to describe quantitatively the evolution in the filament profile, and to separate different stages of extension depending on the total deformation. Theory shows the dramatic difference in the behavior of Newtonian and viscoelastic fluids and this difference depends on the Deborah Number *De*. It turns out that at $De > 0.5$ the fluid behavior is very close to the results presented in Fig. 1. The threshold deformation, corresponding to a change in the slope of the time dependence of the mid-point radius of a filament, was calculated numerically and equaled 0.2. The difference between this value and the value 0.5, found for melts (Fig. 4), may be explained by the difference in the rheological properties of a melt and a solution, as well as by the difference in the experimental schemes used. Meanwhile, experimental data show that strong growth of the normal stresses occurs for *De* or strains in the range of values of 1–2 [108] that corresponds to the rubbery-like state in Fig. 1.

Thus, the Oldroyd model describes the basic effects typical for viscoelastic fluids such as a possibility of storage of the elastic energy at high deformation rates, as well as the relaxation of the accumulated elastic deformations. The ratio of relaxation time and rate of deformation plays a key role in the process under discussion. According to this model, the shape of the bridge looks like a continuously thinning cylinder. If a bridge is formed by a Newtonian fluid, the time dependence of its diameter is linear, while for a viscoelastic (Oldroid) fluid, this dependence is expected to be exponential [13]. Besides, note that the bridge failure of a Newtonian liquid occurs very quickly, while the elastic fluid can be drawn without failure for long time with formation of a long filament. It was proposed to use this experimental protocol for determination of the material constants of a fluid [13]. The main limitation of the Oldroyd model is that in the framework of this model a filament possesses unlimited extensibility. This prediction evidently contradicts experimental facts and that have been accommodated in more complicated rheological models.

The classical linear stability analysis demonstrates that a viscoelastic fluid flow should be more unstable than a Newtonian fluid [116]. Thus, the formation of a stable beads-on-a-string morphology in uniaxial stretching of a viscoelastic thread is inherently a nonlinear dynamic process, accompanied with exponential growth of stresses.

Numerical simulation shows a possibility of the formation of an axially uniform thread connecting two droplets [117].

In the *FENE model*, the constitutive equation takes into account the limited extensibility of a filament, imposing a characteristic finite extensibility factor *L*. This value is understood as the ratio of a completely extended polymer chain to its equilibrium length treating a chain as a dumbbell (as in the Oldroyd model). This parameter creates non-linearity in the *FENE model*, modifying the elastic contribution to the total stress, and if $L\rightarrow\infty$, we come back to the Oldroyd model.

The input of polymer to the stress tensor is expressed as [27]

$$\sigma = Gf(R)\cdot(\mathbf{A}-\mathbf{I}), \tag{9}$$

where G is the elastic modulus, R is the filament radius, $f(R)$ is the factor taking into account the finite extensibility of a polymer chain, and $\mathbf{A}$ is the conformation tensor. The function $f(R)$ is expressed as

$$f(R) = \frac{1}{1-R/L^2} \tag{10}$$

The analysis on the base of the *FENE model* allows us to associate experimental results with the molecular parameters of the system, because L is directly expressed via the polymer molecular weight.

The non-linear Giesekus constitutive equation results in the following equations for the elastic contribution to normal stress in extension σ_{zz} [107]

$$\sigma_{zz} + De\left(\frac{\partial\sigma_{zz}}{\partial t} + v\frac{\partial\sigma_{zz}}{\partial z} - 2\frac{\partial v}{\partial\sigma_{zz}}\right) + \frac{\alpha De}{Oh}\sigma_{zz}^2 = 2Oh\frac{\partial v}{\partial z}, \tag{11}$$

where *De* and *Oh* are the Deborah and Ohnesorge Numbers, respectively (as defined above). A non-linear parameter α is the additional factor compared with the Oldroyd model (for the latter, $\alpha = 0$).

There are several publications devoted to numerical simulations on the base of either *FENE* or *Geisekus* models, and having the goal to describe the time evolution of the filament diameter, and the final breakup of a jet.

Indeed, non-linear models with appropriate choice of the non-linearity parameter provide much better correlation with experimental data in comparison with exponential decay predicted by Eq. (8) [27,114].

3.4. Instability in extension of polymer solutions – phase separation

Even if the polymer concentration along and across a filament is initially homogenous, different physical processes (including solvent evaporation) occurring in a polymer solution under strong extension can result in the redistribution of the homogeneous concentration profile, and, possibly, to the stress-induced phase separation.

The change of solubility in polymer solutions under external forces is a well-known phenomenon [118,119]. This effect, as a rule resulting in crystallization, has been carefully described for shear and extension in many publications (see, for example, [120–127]). A similar effect is known for the amorphous phase separation [114]. Note that extension is much more effective than shear in promoting phase separation [122,125,127].

Phase separation in extension, being accompanied by the formation of rather big drops on a stretched filament and by "solidification" of a fiber, formed from moderately concentrated solutions, was described in pioneering publications [128,129]. The formation of solid fibers as a result of the phase separation in a dilute solution flow was carefully studied and described in the latest publications [130,131]. This effect was called "blistering" and connected with the formation of nanofibers [131]. The detailed analysis made in these publications has shown that evaporation does not play a significant role in this phenomenon. Phase separation was related to the ultimate degree of polymer chain orientation and was treated as the final stage of capillary breakup. According to the proposed instability mechanism, considered as the elongation-induced phase separation, a solvent forms a thin liquid cylinder on a filament surface. Thereafter, this liquid film starts to move along the surface under capillary and gravity forces that finally result in the formation of droplets.

The detailed picture of the initial stage of solvent ousting from a filament, as well as the formation of a liquid cover on a filament before its transformation into droplets, are shown in Fig. 11a; and the complete sequence of events is presented in Fig. 11b.

Possibly, the first mathematical examination of the drawing of a thin film along a flat surface was performed by Kapitsa [132] (cited according to [133]). The motion is the result of a balance between the droplet weight, viscous stresses, and surface tension. The main result of this work is the explanation of the formation of the steady wave structure on a surface. Such a structure, called unduloid, is usually characterized by formation of a liquid bridge. Modern situation in examining of this problem is reviewed in [134,135]. A similar pattern is described for liquid film, draining on a cylindrical thread surface [136]. It is also of high importance that in a long-term range the droplets lose some mass through the fiber coating, which decreases their velocity [137].

A possibility of "blistering" was explained by the finite extensibility of macromolecular chains as a mechanism for phase separation [131]. Consequently, the mathematical description of this effect should be based on the nonlinear *Giesekus* or *FENE* models (see Section 3.3). It seems that there is a difference in principle in the instability phenomenon between *bead-on-a-string* patterns due primarily to capillary forces in a single-phase solution and *blistering*, i.e., formation of separate solvent drops due to strong concentration redistribution (possible phase separation) and a transition to a two-phase system. As mentioned above, the beads-on-a string filament structure is generally understood as droplets, interconnected by long thin fluid ligaments [22]. It implies that beads and thin filaments constitute a single object. As discussed above, numerous mathematical modeling exercises treat this object as a homogeneous medium, described by some constitutive equation. However, it has been proven that in at least at some cases phase separation happens and this phenomenon by itself leads to *blistering* [130]. In such a case it is reasonable to ask: where is the separation line

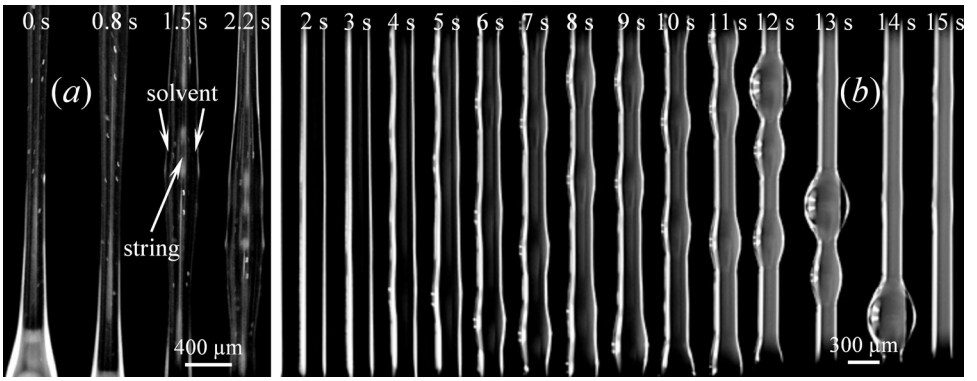

Fig. 11. Consecutive stages of "phase separation", accompanied by formation of near-surface solvent layer (a) and appearance of separate drops (b). The full observation time was 16 s. Noticeable waves appear at the 4th second; droplets are uniting with their neighbors and are forming larger droplets at the 7th second; the large drop is moving downwards along a string, collecting all solvent at the 15th second. Formation of separate droplets on an oriented polymer fiber. Polyacrylonitrile, $\bar{M}_W = 94.6 \times 10^3$. The solvent is dimethyl sulfoxide, solution concentration is 15%, and $T = 20\,^{\circ}C$ [93].

and transition between these two effects making them different? It is rather dangerous to draw a conclusion only on the base of a visual estimation of the structural appearance because the beads on a string and the separated drops look the same. So, one can suppose that so-called beads-on-a-string phenomenon, in reality, is always (or almost always) not droplets interconnected by ligaments but drops detached from a string and forming a separate phase. It is interesting to notice that the original pattern of "bead-on-a-string" shown in Fig. 10 (adopted from [104]) was also reproduced in a review [3] and the effect was called "blistering" without distinguishing the phenomena.

Perhaps it is more correct to speak about continuous transition from beads, composing the same construction with an oriented polymer string, to formation of a liquid layer at a central core and further droplet separation from a central fiber. One can observe the appearance of a solvent cover on a filament (Fig. 11a) and transformation of this cover into separate drops (Fig. 11b). Fig. 11 clearly demonstrates consecutive stages of this phenomenon which, possibly, becomes more evident in the case of more concentrated solutions and thicker filaments. However, additional arguments are needed to clarify the situation concerning equivalence or difference of these two mechanisms of instability and a boundary between them.

The fact that the sample during elongational flow becomes inhomogeneous is of high importance for modeling of this process. So the temporal and spatial composition evolution occurs in strong flows resulting in changes of material properties along and across a filament. We suppose that this should be taken into account in formulation of the governing field equations; in doing so a filament should not be considered as a single-phase medium.

3.5. Electrospinning

Very high elongation rates of polymer solutions can be created by application of sufficiently high voltage to a polymer solution droplet. A liquid becomes charged and electrostatic repulsion, counteracting the surface tension, forces the droplet to stretch. At some critical point, liquid erupts from the droplet surface, and a charged liquid jet is formed which, in turn, can be transformed into thin fiber.

Such a process, called electrospinning, is an effective technological method for nanofiber fabrication allowing fiber diameters of about 50–500 nm, several orders of magnitude smaller than the diameter of the orifice, and well below the diameter of conventional extruded fibers (10–100 μm).

The physical principles of electrospinning are based on the Taylor examination, related to a specific problem of fluid mechanics [138–140]. In particular, Taylor showed that a viscous fluid is in equilibrium under an electric field when a jet leaving an orifice has the form of a cone (so-called Taylor cone) with a semi-vertical angle equal to 49.3° [141]. The initial phase of the thin fiber formation is shown in Fig. 12. The fluid is going out of a nozzle, forming the Taylor cone which, in turn, is being transformed via the transition zone into a jet.

The principal stages of the electrospinning process are shown in Fig. 13. Polymer solution, typically semi-dilute in nature, is extruded from a spinneret, and by a strong

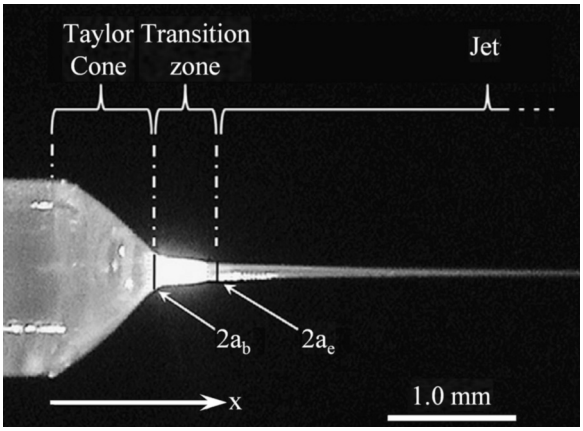

Fig. 12. Taylor cone zone, with the transition zone, and the beginning of the thin jet in an electrically driven jet. The cross-sectional radii at the beginning and end of the transition zone are denoted a_b and a_e, respectively [150].

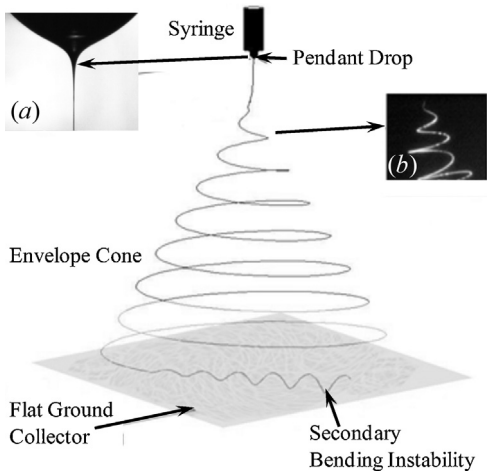

Fig. 13. Sketch of the electrospinning process (a) image of the Taylor cone and (b) image of the bending instabilities [142].

electric field a jet is formed at the tip (see Fig. 13a). The resulting jet then undergoes extreme elongation and thinning, of the order of 10^5, accompanied by a strain rate of the order $10^3\ s^{-1}$, leading to stretching and orientation of the polymer chains (Fig. 13b). Due to extremely rapid solvent evaporation the solidification of the jet occurs, and the fiber formed achieves the collector plate, being almost completely free of a solvent in spite of the fact that the process duration is within 10^{-2} s.

Several comprehensive reviews devoted to the electrospinning process have been published (only five of many are cited as examples [142–147]). In this review we would like to focus on the basic aspects of electrospinning, which are related to the theme of the discussion, namely, the behavior of a jet of polymer solution under high elongation rates (as was mentioned above, the deformation rates in electrospinning can reach $10^3\ s^{-1}$).

This problem can be analyzed both from the macroscopic and from the microscopic point of view. In the latter case (microscopic level) a modification in the polymer matrix state (in particular, the orientational ordering of macromolecules [148]) is examined. The macroscopic point of view allows one to describe the hydrodynamic evolution of the jet.

Under the electric field the solution jet is moving with acceleration, so that the local velocity contains both longitudinal and radial components [149]:

$$v_z \approx v_0\left(1+\frac{z}{z_0}\right)^2+\ldots, \quad v_r \approx -v_0\left(1+\frac{z}{z_0}\right)\frac{r}{z_0}+\ldots, \quad (12)$$

therefore, the jet takes on an hyperbolic form:

$$r_J(z) \approx \frac{r_0}{1+z/z_0}, \quad (13)$$

where v_0 is the jet initial velocity, and r_{J0} is the jet initial radius. The characteristic length z_0 determines the scale of velocity increase, and depends on the flow rate, viscosity, electric field and electric conductivity of the solution.

This theoretical result is in good agreement with experimental observations. Several optical methods have been used to characterize electrospinning jets, ranging from simple low speed or static white light imaging of the jet profile near the tip to more complex techniques such as high speed bright-field imaging of unique formations in the jet, and laser Doppler velocimetry, fluorescence microscopy, etc.

For example, the velocity measurements presented by Han et al. [150] are demonstrated in Fig. 14a. The liquid solvent accelerates rapidly, moving away from the beginning of the jet, and at a distance 6 mm from the starting point its velocity achieves 1 m/s. In doing so, the stretching rate in the transition zone dV/dx lies in the range 100–1000 s^{-1}. The jet diameter decreases also very sharply and it is too small for a measurement at distances exceeding 3 mm (see Fig. 14a).

Analogous results were obtained by Bellan et al. [151] (see Fig. 14b): at a distance of 1 mm from the starting point the solvent velocity achieves 0.25 m/s, and such acceleration corresponds to the stretching rate of about 300 s^{-1}.

It is clear that the velocity profile reproduced above demonstrating rapid unlimited increase in the longitudinal velocity (see Fig. 14), can be accepted as a satisfactory approximation only in the beginning of the spinning jet. The point is that the electrospinning process is accompanied by significant mass loss due to extremely rapid solvent evaporation occurring with continued jet flow [9,31,152–154], so the solution properties are substantially

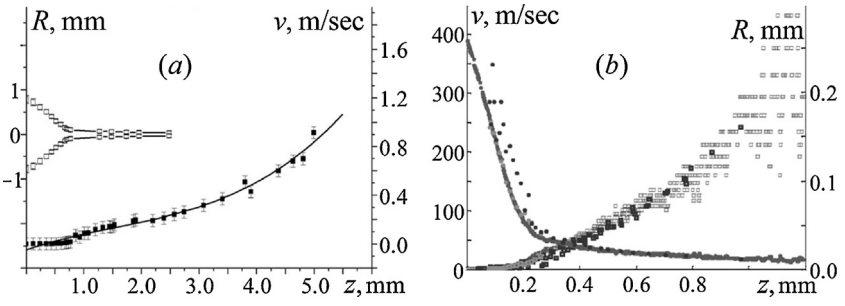

Fig. 14. (a) Profile of the transition zone following the modified Taylor cone and the beginning of the jet. The cross-sectional radius is shown as $R = R(z)$ [150]; and (b) Velocity and jet radius plotted as a function of z position (length along the jet) (b – Reproduced with permission from Bellan et al. [151]), Copyright 2007. Reproduced with permission from AIP Publishing LLC.

modified along the jet. Due to solvent evaporation the solution viscosity sharply increases, and in the end the jet solidifies. The stretching of the filament also affects the viscoelasticity of the polymer solution (see below). As a result the increase in the longitudinal velocity, v_z, slows down; and, finally, it tends to saturation: $v_z \to v_\infty$. In this case the radial velocity, v_r, tends to zero, whereas the filament radius stops decreasing and tends to its final value $r_j^{(\infty)}$. The effect of the evaporation rate on the final radius value of electrospun nanofibers and their properties was studied experimentally [155].

Note that in general the electrospinning process is unstable and can be stabilized only in certain parameter region, whereby the stable zone of the process is rather narrow [156]. Particularly, electrospinning can be accompanied by a fiber failure, caused by a filament fracture due to capillary wave breakup (Rayleigh instability) or/and by breakage of the fiber due to the stresses overcoming some limiting tensile strength (necking, rupture) [157]. As a result, in place of continuous filament being transformed into fiber, a spray forms. Such a process is called electrospraying, and historically just electrospraying precedes electrospinning process [158–163].

Nevertheless, in spite of the abovementioned capillary breakup, the stable (from a technological point of view) electrospinning process resulting in formation of nanofibers, is possible at certain conditions for many polymer solutions and even melts.

At the same time the other instability type of a spinning jet, related to its form, i.e., the bending instability of a jet that does not result in the fiber failure is also possible [164,165]. The detailed analysis of possible instabilities of such a type is presented by Reneker and Yarin in their review [147].

The first is the bending instability. After the jet flows away from the droplet in a nearly straight line (see Fig. 13a), it bends into a three-dimensional coil, passing into the whip-like movement of a jet (see Fig. 13b). After several turns are formed, a new electrical bending instability forms a smaller coil on a turn of the larger coil. This type of instability arises due to rapid growth of bending perturbations under the influence of the charge carried with the jet [147,164,165]. Note that this bending instability does not result in electrospun nanofiber failures, and from the point of view of the problem in question has no interest. The branching of spinning jet that occurs under some circumstances is also beyond the framework of our consideration.

The general model for steady elecrospinning of a Newtonian liquid taking into account viscous, electrical, surface tension and inertial forces was formulated in [141]. Further analysis of dynamic equations showed that besides the classical axisymmetrical Rayleigh-type instability, the nonaxisymmetric (also called whipping) instability appears due to bending forces and this phenomenon plays the key role in the mechanism of filament thinning and consequently, polymer orientation [166,167]. The macromolecule orientation arising in electrospun nanofibers as a result of stretching during spinning, has been demonstrated by several researchers (see, for example, [168–171]).

It is appropriate also to mention the scaling approach to the hydrodynamic analysis of electro-charged jets [172,173], which has experimental confirmation [174].

The hydrodynamic approach makes it possible also to take into account the elasticity of polymer solutions. And the elasticity of polymer solutions results in the bending instability of the spinning jet discussed above [147,164,165]. But more detailed analysis shows that the polymer solution elasticity is the key point in electrospinning process, and the general belief is that only elastic forces can stabilize the jet, suppressing the Rayleigh-type instability, and preventing fiber failures, in particular, the capillary breakup of the spinning jet [175]. In particular, Han et al. showed that the straight sections are stabilized by the high initial longitudinal stresses in the jet generated due to strong electrically driven stretching in the transition zone [150]. Nevertheless, up to now the effect of the polymer jet elasticity under high stretching has been insufficiently and incompletely studied, and, in our opinion, it requires further examination.

Up to now only the macroscopic level of the analysis was discussed, referring to but a portion of the huge number of the published papers. Few research studies are devoted to the microscopic level of the problem in question. In these studies the structure and the state of the polymer matrix of electrospun nanofibers are analyzed, utilizing birefringence [171,176], Raman techniques [168,169], and transmission electron microscopy [170]. The main outcome of these studies is that the extreme elongation of the spinning jet leads to stretching and orientation of the polymer chains inside electrospun nanofibers, as was mentioned above (see, [168–171]). It is this phenomenon (macromolecule orientation due to the jet stretching) that is of most interest for us. Unfortunately, these data reveals only the final state of the system in question; in doing so the partial non-controlled relaxation of a non-equilibrium state of the polymer matrix within electrospun nanofibers occurs. In other words, the information related to the state of polymer at extreme elongation is partially lost.

A recent study, based on the fast *X*-ray phase-contrast imaging, allows one to analyze the on-line evolution of polymer system inside the spinning jet [95,177]. This study focuses on the dynamics of a highly entangled semi-dilute polymer solution under extreme longitudinal acceleration (note that the spinnable polymer solutions are semi-dilute, highly entangled [178]). The polymeric topological network can be approximated by a lattice model of "beads" and linear "springs," similar to the Rouse chain relaxation model. The "beads" (nodes) representing a topological knot are connected by springs, polymer sub-chains, and have an effective sub-chain mass m. Each node bears a hydrodynamic force proportional to the sub-chain effective size $a_{eff} \propto aN_s = N(c/c^*)$, as well as entropic elastic forces from its neighbors. Gaussian chain statistics is assumed, leading to a linear force-elongation relationship.

The theoretical modeling, taking into account the elasticity of polymer network, hydrodynamic interaction between solvent and macromolecules, and inertial forces, predicts substantial longitudinal stretching and transversal contraction of the polymer network [177].

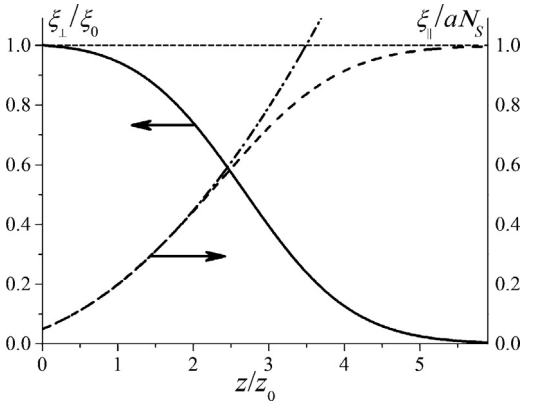

Fig. 15. Polymer network conformation. Relative radial contraction, $\xi_\perp/\xi_0$ (solid line), and relative axial stretching, $\xi_\parallel/aN_s$ (dashed and dot-dashed lines), versus the relative axial position, z/z_0. The results were obtained by the simulation (dashed and solid lines) and theoretical model (dot-dashed line). Parameters are: $N_s = 400$, $\alpha = 1000$, and $\beta = 0.3$ [177].

The stretched mesh size $\xi_\parallel(\hat{z})$, in the direction of the jet can be estimated in a $1/\alpha$ approximation as follows:

$$\frac{\xi_\parallel(\hat{z})}{\xi_0} \approx \frac{\hat{v}_z(\hat{z})}{1+(1/\alpha)[d\hat{v}_z(\hat{z})/d\hat{z}]}, \tag{14}$$

where $\alpha = z_0 v_0 a_{eff}\eta/m(v_0^2 - c_{net}^2)$ is a dimensionless parameter, and $\hat{v}_z(\hat{z}) \equiv v_z(z)/v_0$, defined in Eq. (12). The parameter $c_{net} = \sqrt{T/m}$ is the "sound" velocity in the polymer network due to entropic elasticity.

The sign of the parameter α, which depends on the sign of the term $(v_0^2 - c_{net}^2)$, and its magnitude, determine the behavior of the system: for $\alpha > 0$ the jet's local velocity is faster than that of the polymer network, and the effect of the hydrodynamic force is dominant; for $\alpha < 0$ the polymer network's local velocity is faster than that of the jet, and the effect of network connectivity is dominant (i.e., stretching is caused by a pull at the far end of the jet). The jet velocity v_z saturates to v_∞ as the stretching ratio converges to $\xi_\parallel/\xi_0 \approx v_\infty/v_0$, confirming that the stretched conformation of the polymer network remains even after velocity saturation.

The dependence $\xi_\parallel/aN_s$ on the position z/z_0 along the jet is shown in Fig. 15 (dot-dashed lines). The theoretical calculations were supported by numerical simulations based on the 3D random walk model under external field (see Fig. 15, dashed lines). The difference between analytical calculations and numerical simulations is observed for the highly stretched state of polymer sub-chains, when the stretching of the polymer sub-chains according to Eq. (14) exceeds the maximal possible elongation corresponding to fully-stretched state, whereas the stretching, calculated on the base of the 3D random walk simulations, tends to saturation.

The hydrodynamic compression of the polymer network in the direction perpendicular to the jet, in each cross-section of the jet, becomes stationary very fast, resulting in the following effective radius of the polymer network

$$r_P(z) \approx \frac{\xi_\perp(z)}{\xi_0}\frac{r_{J0}}{1+z/z_0} = \frac{\xi_\perp(z)}{\xi_0} r_J(z), \tag{15}$$

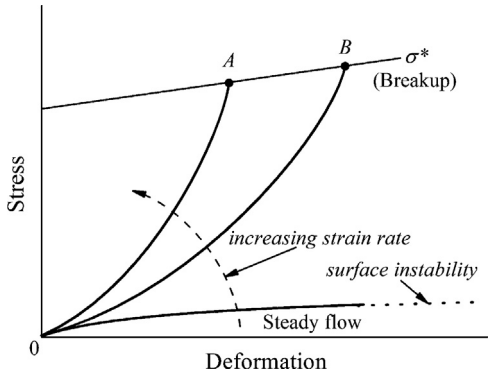

Fig. 16. Deformation behavior of entangled polymer melts and solutions in the rubbery-like state.

where r_{J0} is the initial radius of the jet, $r_J(z)$ is determined by Eq. (13), the parametric dependence $\xi_\perp(z)$ (see Fig. 13, solid line) is calculated as a function of $\xi_\parallel(z)$ as

$$\frac{\xi_\perp}{\xi_0} \cong \frac{3}{2+1/\sqrt{1-(a\xi_\parallel/\xi_0^2)^2}}, \quad \xi_\parallel \sim aN_s \tag{16}$$

Thus, the radial hydrodynamic forces compress the polymer network into a hyperbolic shape, while the stretching forces reduce its radius further.

Note that the transformation of sub-chains from a coil-like equilibrium state into a stretched state occurs as a continuous crossover, and no phase transition is observed, in contrast to the well-known coil-stretch transition, described by de Gennes [179]. Unlike stretching of an individual chain, locally the dominant force that provides network transformation during its stretching is the elastic force, whereas the hydrodynamic forces give rise to the global stretching of the network. As a result, the network sub-chains are subjected to the action of the network portion situated farther along the jet, i.e., of a force, independent of local stretching. In contrast, the force acting on an individual polymer chain under an ultrahigh velocity gradient increases with macromolecule stretching. Similar behavior, continuous crossover from a coil-like state into a stretched state, was observed upon examination of the state of an individual macromolecule under external force acting on its ends [180].

The above theoretical analysis attained experimental validation on the base of *X*-ray phase-contrast imaging of electrospinning jets of poly(ethylene oxide) and poly(methyl methacrylate) semi-dilute solutions presented in the same paper [177].

Thus, the electrospinning process allows one to create the experimental conditions that provide an extreme stretching of a polymer jet, in doing so the equipment required for this goal is simple enough.

4. Physics of extension

The scheme of polymer deformation behavior in extension can be presented as shown in Fig. 16. It corresponds to the master curve in Fig. 1, at least in the rubber-like state. The positions of the limiting points (black circles *A* and *B*

in Fig. 16) are presented in Figs. 1 and 4 as functions of the deformation rate.

Now let us focus on the dependencies "stress versus deformation" – curves 0*A* or 0*B* in Fig. 16. It would be natural to treat these curves in the framework of the classical theory of rubbery elasticity [181,182]. Therefore, the $\sigma(\varepsilon_{el})$ dependence should be described by the equation

$$\sigma = \frac{E}{3}\left(\lambda^2 - \frac{1}{\lambda}\right), \tag{17}$$

where E is the initial (linear) elastic modulus.

The classical model of rubbery elasticity assumes the affine deformation of a network (formed by either chemical bonds or entanglements), and in the case of linear polymers no disentanglements occur.

However, this model does not satisfy experimental data in the following aspects. This is essentially an equilibrium model, and it does not presume any time effects, existing in any case, because, it is quite evident, the strain rate affects the experimental results. Besides, it is well known that this model diverges from experimental data at high draw ratios.

It is reasonable then to discuss the physics of stretching in the framework of the popular tube model, proposed by Edwards in an early model for the trapped entanglements in a rubber network [183,184]. The tube model is frequently treated as the key point of the modern theory of polymer rheology [185–189]. According to the concept of the tube model, surrounding chains restrict the transverse motion of a polymer, so that each polymer macromolecule is effectively confined to a tube-like region. That means that the dynamics of polymer macromolecules can be modeled by considering a probe chain repeating along its backbone in a tube formed by molecular surrounding (mean-field approximation). The test chain can execute barrier-free motions inside the tube at the time scale below the Rouse time τ_R.

In the case of slow deformations (the deformation rates should be lower than $1/\tau_R$, i.e., lower than the reptation rate), the chain does not stretch! The relaxation spectrum of a chain inside a tube is expressed by the Rouse law: $\tau_n = \tau_d/n$, where τ_d is the second characteristic relaxation time (longest relaxation time) determined by the full chain length [186].

At the same time, the level of deformation also affects the polymer dynamics. The point is that macroscopic deformations of the polymer system are accompanied by modifications in macromolecular conformations (in particular, stretching of polymer results in extended macromolecule conformations). In the tube model, the conformation state of macromolecules is characterized by the single-segment correlation function $S_{\alpha\beta}(n,n') = \left\langle \frac{\partial R_\alpha(n,t)}{\partial n}\frac{\partial R_\beta(n',t)}{\partial n'} \right\rangle$ averaging the orientation of all segments in a probe chain, confined in the tube, where $\mathbf{R}(s,t)$ is a position of a tube segment s at the time moment, t, and the local stress tensor $\sigma_{\alpha\beta}$ is being determined by this configuration of the probe chain $\mathbf{R}(s,t)$ [179]. More exactly, the local stress tensor $\sigma_{\alpha\beta}$ is proportional to the correlation function $S_{\alpha\beta}(n,n')$: $\sigma_{\alpha\beta} = c_{Ch}(3k_BT/a^2)\,S_{\alpha\beta}(n,n')$ (here c_{Ch} is the polymer chain concentration, and a is the tube diameter) [186,188].

The general tube model predicts that for the steady-state relatively slow flows of entangled linear polymers, the stress increases proportionally to an increase of the deformation rate, i.e., the behavior of a melt is linear (in case of very high flow rates, no steady-state regime is possible). The issue related to the behavior of a chain at high strain rates exceeding $1/\tau_d$ (or at high stresses) is of highest interest. The theoretical analysis of shear flows for monodisperse polymers forecasts a sharp increase of shear rate (drop of the apparent viscosity) [185], while one can expect the transition from fluid to shear-induced rubber-like state with loss of fluidity [31]. This phenomenon is quite similar to the transition to rubber-like state in extension, shown in Fig. 1.

Concerning fast elongational flows, we should presume that when the deformation rate noticeably exceeds $1/\tau_d$, reptations become frozen, and the chains remain trapped inside the tube.

On the other hand, a successful theory of polymer rheology, derived from the tube model, includes the assumptions that both the entanglement length and tube diameter decrease with chain stretching [189]. The effect of chain stretching on the tube characteristics (tube diameter, tube persistence length and tube hops resulting in its form modification) was analyzed in [190] (these tube parameters were scaled by the power law). It turned out that this renormalization affects the macroscopic system behavior only in the case of high enough shear rates when $\dot{\varepsilon}\tau_s > 1$ (τ_s is the stretching time of the polymer chains). Unfortunately, the model does not predict the exponent values, which might be compared with the experiment.

More detailed information regarding the modification of the tube parameters can be obtained by the numerical methods. The Monte Carlo simulations show that under uniform tension the tube diameter equals its unperturbed value a when the pulling force F is less than the thermal tension k_BT/a, and scales as $F^{-1/3}$ when F exceeds k_BT/a; and when the tension is large enough to nearly fully extend the chain, decrease of the tube diameter becomes stronger: it scales as $F^{-2/3}$ [191].

As a general rule, the tube model based molecular consideration does not provide clear predictions for the rheological behavior of linear polymer melts in extension except in the rather evident case of slow flows.

In [192], the stochastic tube model was proposed and later modified in [193] by including a configuration-dependent friction coefficient (as was first proposed by Giesekus many years ago [194]). It is important that this model discusses situations far from equilibrium and especially for fast flows. At the same time, the above mentioned stochastic tube model describes only disentanglement of the polymer system, caused by high shear rate of the flow; whereas the suppression of reptation mobility which results in the "spurt" (flow stopping), remains beyond of the framework of the model.

Transition of the polymer liquid to the rubber-like deformation behavior under high deformation rate (as well as the "spurt" phenomenon) is caused by the suppression of disentanglement of macromolecules when the reptation mobility is frozen. This transition occurs when the elastic energy of deformed entanglement length (a subchain

between two neighbor entanglements) exceeds the thermal energy: $(\sigma_{Sh}^2/2G) > (m_e/\rho)k_BT$, here σ_{Sh} is the shear stress corresponding to the deformation-induced transition from the flow to the rubber-like state, G is the shear modulus, m_e is the mass of the subchain between two neighboring entanglements, ρ is polymer density, T is the absolute temperature, and k_B is the Boltzmann constant [46].

Note that in the case of such high stretching levels, when the reptation mobility is suppressed, the disentanglement (if it occurs) should be provided by the alternative mechanism of the deterministic movement of macromolecules which results in their pulling out of entanglement knots.

5. Conclusion

Systematic examination of uniaxial extension of polymeric filaments, made of melts or of semi-dilute entangled solutions, has demonstrated that the dominant factor peculiar to liquid polymer systems is their rubber-like elasticity, superimposed on viscous flow. Generally, the spatial-temporal evolution and stability of a viscoelastic filament are determined by the viscous, elastic and surface properties of a fluid, as well as by its relaxation ability.

In case of low deformation rates, the viscous (irreversible) deformations prevail and very large strains (flow) are possible. In this low strain rate domain, possible instability is completely due to surface tension. With the increase in deformation rate, elastic deformations increase, giving rise to competition between viscous flow and elastic deformation, and, finally, elasticity becomes dominant due to the fact that the relaxation does not have enough time to occur (reciprocal deformation rate becomes less than relaxation time). Then the further extension of a specimen occurs according to the mechanism of rubbery deformations (like stretching of an elastic strip) with neglecting flow. Such behavior can be treated as the deformation-induced *flow-to-rubbery transition*. This phenomenon is especially evident in extension of homogeneous monodisperse polymers though similar effect takes place in polydisperse polymers too.

The process continues up to the complete uncoiling (continuous transition in place of the phase coil – stretched transition) of macromolecules. Transient elastic deformation and the degree of the macromolecule extension are determined by deformation rates. Just the elasticity of a liquid (but not the elongation viscosity growth) stabilizes a filament at high deformation rates.

In the case of fast stretching of dilute polymer solutions, instability of a filament is initiated by capillary forces and develops according to the Rayleigh-Plateau mechanism. However, this instability in semi-dilute entangled solutions can be suppressed by elasticity of the polymer network existing in a polymer solution. Nevertheless, in the case of fast flows of polymer solutions, a solvent can exude from a macromolecular network due to its contraction or due to the loss of solubility of highly oriented macromolecules. As a result, a radial solvent gradient appears. This phenomenon leads to formation of pure solvent drops on the surface of the highly oriented filament and can be treated as elongation-induced phase separation. Effects of such a kind are especially strongly pronounced in electrospinning processes, where effective stretching is achieved by application of the electrical field.

Phenomenological description of the polymer solution behavior in extension is usually based on some non-linear constitutive rheological models taking into account limited extensibility of macromolecular chains. This approach allows for prediction (at least qualitatively) of the main effects observed in stretching of polymer solutions. However this approach seems to be limited and insufficient because this concept utilizes some unchanging parameters of a medium, and does not take into account the evident evolution of concentration both along and across a filament that results in spatial and temporal modifications of rheological properties of a medium.

Acknowledgment

Authors acknowledge financial support from the Russian Foundation for Basic Research through Grant no. 13-03-00016.

References

[1] Plateau JAF. Statique experimentale et theorique des liquides soumis aux seules forces moleculaires. Paris: Gauthiers-Villars; 1873, 495 pp.
[2] Rayleigh L. On the instability of jets. Proc London Math Soc 1878;10:4–13.
[3] Eggers J, Villermeau E. Physics of liquid jets. Rep Prog Phys 2008;71, 03660/179.
[4] Malkin AYa, Semakov AV, Kulichikhin VG. Self-organization in the flow of complex fluids (colloid and polymer systems). Part 1. Experimental evidence. Adv Colloid Interface Sci 2010;157:75–90.
[5] Subbotin AV, Malkin AYa, Kulichikhin VG. Self-organization in the flow of complex fluids (colloid and polymer systems). Part 2. Theoretical model. Adv Colloid Interface Sci 2011;162:29–38.
[6] Malkin AYa, Isayev A. Rheology. Concepts, methods and application. 2nd ed. Toronto: ChemTec Publ.; 2012, 528 pp.
[7] Matta JE, Tytus RP. Liquid-stretching using a falling cylinder. J Non Newton Fluid Mech 1990;35:215–29.
[8] Bazilevsky AV, Entov VM, Rozhkov AN. Orientational effects in the decomposition of streams and strands of diluted polymer solutions. Sov Phys Dokl 1981;26:333–5 [Rep USSR Acad Sci 257: (1981) 336–9].
[9] Bazilevsky AV, Entov VM, Rozhkov AN, Yarin AL. Polymeric jets beads-on-string breakup and related phenomena. In: Oliver DR, editor. Proceedings of the third European rheology conference and golden jubilee meeting of the British society of rheology. Amsterdam: Elsevier Ltd.; 1990. p. 41–3.
[10] Tirtaatmadja V, Sridhar T. A filament stretching device for measurement of extensional viscosity. J Rheol 1993;37:1081–102.
[11] Bazilevsky AV, Entov VM, Lerner MM, Rozhkov AN. Failure of polymer solution filaments. Polym Sci A 1997;39:316–24 [Vysokomol Soedin A 1997;39:474–82].
[12] Szabo P. Transient filament stretching rheometer. I. Force balance analysis. Rheol Acta 1997;36:277–84.
[13] Entov VM, Hinch EJ. The effect of a spectrum of relaxation times on the capillary thinning of a filament of elastic liquid. J Non Newton Fluid Mech 1997;72:31–54.
[14] Anna SL, Rogers Ch, McKinley GH. On controlling the kinematics of a filament stretching rheometer using a real-time active control mechanism. J Non Newton Fluid Mech 1999;89:307–35.
[15] Steller M, Brenn G, Yarin AL, Sigh RP, Durst F. Validation and application of a novel elongational device for polymer solutions. J Rheol 2000;44:595–616.
[16] Anna SI, McKinley GN. Elastic-capillary thinning and breakup of model elastic liquids. J Rheol 2001;45:115–38.
[17] Bazilevsky AV, Entov VM, Rozhkov AN. Failure of the Oldroyd liquid bridge as a method for testing the rhological properties of polymer solutions. Polym Sci A 2001;43:716–26 [Vysokomol Soedin A 2001; 43: 1151–72].

[18] Rothstein JP, McKinley GH. Inhomogeneous transient uniaxial extensional rheometry. J Rheol 2002;46:1419–45.
[19] Czabo P, McKinley GH, Clasen Ch. Constant force extensional rheo metry of polymer solutions. J Non Newton Fluid Mech 2012;169–170:26–41.
[20] Martinie L, Buggisch H, Willenbacher N. Apparent elongational yield stress of soft matter. J Rheol 2013;57:627–46.
[21] McKinley GH. Visco-elastic-capillary thinning and break-up of complex fluids. In: Bindings DM, Walters K, editors. Rheology reviews. Nuneaton: The British Society of Rheology; 2005. p. 1–48.
[22] Olivera MSN, Yeh R, McKinley GH. Iterated stretching, extensional rheology, and formation of beads-on-a-string structures in polymer solutions. J Non Newton Fluid Mech 2006;137:137–48.
[23] Clasen C, Plog JP, Kulicke WM, Owens M, Macosko C, Scriven LE, Verani MM, McKinley GH. How dilute are dilute solutions in extensional flows? J Rheol 2006;50:849–81.
[24] Tuladhar TR, Mackley MR. Filament stretching rheometry and break-up behaviour of low viscosity polymer solutions and inkjet fluids. J Non Newton Fluid Mech 2008;148:97–108.
[25] Arnolds O, Buggisch H, Sachsenheimer D, Willembacher N. Capillary breakup extensional rheometry (CaBER) on semi-dilute and concentrated polyethyleneoxide (PEO) solutions. Rheol Acta 2010;49:1207–17.
[26] Niedzwiedz K, Buggisch H, Willenbacher N. Extensional rheology of concentrated emulsions as probed by capillary breakup elongational rheometry (CaBER). Rheol Acta 2010;49:1103–16.
[27] Vadillo DC, Tembely M, Morrison NF, Harlen OG, Mackley MR, Soucemarianadin A. The matching of polymer solution fast filament stretching, relaxation, experimental results with 1D and 2D numerical viscoelastic simulation, and break up. J Rheol 2012;56:1491–516.
[28] Sentmanat ML. Miniature universal testing platform, from extensional melt rheology to solid-state deformation behavior. Rheol Acta 2004;43:657–69.
[29] Sentmanat ML, Wang BN, McKinley CH. Measuring the transient extensional rheology of polyethylene melts using the SER universal testing platform. J Rheol 2005;49:585–606.
[30] Vinogradov GV, Malkin AYa, Volosevitch VV, Shatalov VP, Yidin VP. Flow, high-elastic (recoverable) deformations and rupture of uncured high molecular weight linear polymers in uniaxial extension. J Polym Sci Polym Phys Ed 1975;13:1721–35.
[31] Vinogradov GV, Malkin AYa, Volosevitch VV. Some fundamental problems in viscoealstic behavior of polymers in shear and extension. Appl Polymer Symp 1975;27:47–59.
[32] Malkin AYa, Vinogradov GV. Fracture of polymers in the visco-fluid state on stretching. Polym Sci USSR 1985;27:245–57 [Vysokomol Soedin A 1985;27: 227–37].
[33] Kurbanaliev MK, Vinogradov GV, Malkin AYa. Rupture of linear polybutadiene above its glass transition in different liquid media. Polym Sci USSR 1982;23:2215–22 [Vysokomol Soedin A 1981;23: 2032–38].
[34] Malkin AYa, Petrie CJS. Some conditions for rupture of polymer liquids in extension. J Rheol 1997;41:1–25.
[35] James DF, Yogachandran N. Filament breaking length – a measure of elasticity in extension. Rheol Acta 2006;46:161–70.
[36] Malkin AYa, Semakov AV, Kulichikhin VG. Entanglement junctions in melts and concentrated solutions of flexible-chain-polymers: macromodeling. Polym Sci A 2011;53:1198–206 [Vysokomol Soedin A 2011;53:2119–28].
[37] Malkin AYa, Semakov AV, Kulichikhin VG. Macroscopic modeling of a single entanglement at high deformation rates of polymer melts. Appl Rheol 2012;22, 32575/1–9.
[38] Smith TR. Ultimate tensile properties of elastomers. II. Comparison of failure envelopes for unfilled vulcanizates. J Appl Phys 1964;35:27–36.
[39] Yoshi YM, Denn MM. Rupture of entangled polymeric liquids in elongational flows. J Rheol 2003;47:291–8.
[40] Yoshi YM, Denn MM. Rupture of entangled polymeric liquids in elongational flows with dissipation. J Rheol 2004;48: 591–8.
[41] Barroso VC, Maia JM. Time dependent effects on the rupture of molten linear polymers in extension. J Non Newton Fluid Mech 2005;126:93–103.
[42] Bailey J. An attempt to correlate some tensile strength measurements on glass III. Glass Ind 1939;20:95–9.
[43] Vinogradov GV, Malkin AYa, Yanovskii YuG, Borisenkova EK, Yarlykov BV, Berezhnaya GV. Viscoelastic properties and flow of narrow distribution polybutadiens and polyisoprenes. J Polym Sci A-2 Polym Phys 1972;10:1061–84.
[44] Vinogradov GV, Malkin AYa. Rheology of polymers. Berlin: Springer; 1980, 467 pp.
[45] Wang SQ, Ravindranath S, Wang YY, Boukany PE. New theoretical considerations in polymer rheology: elastic breakdown of chain entanglement network. J Chem Phys 2007;127, 064903/1–14.
[46] Malkin AYa, Semakov AV, Kulichikhin VG. Modeling macromolecular movement in polymer melts and its relation to non-linear rheology. Rheol Acta 2011;50:485–9.
[47] Zhu X, Wang SQ. Mechanisms for different failure modes in startup uniaxial extension: tensile (rupture-like) failure and necking. J Rheol 2013;57:223–48.
[48] Wang YY, Wang SQ. From elastic deformation to terminal flow of a monodisperse entangled melt in uniaxial extension. J Rheol 2008;52:1275–90.
[49] Ianniruberto G, Marrucci G. Entangled melts of branched PS behave like linear PS in the steady state of fast elongational flows. Macromolecules 2013;46:267–75.
[50] Meissner J. Elongation behavior of polyethylene melts. Rheol Acta 1971;10:230–42.
[51] Rolón-Garrido VH, Wagner MH. The damping function in rheology. Rheol Acta 2009;48:245–84.
[52] Abo J, Rolón-Garrido VH, Wagner MH. Extensional viscosity in uniaxial extension and contract flow – comparison of experimental methods and application of the molecular stress function model. J Non Newton Fluid Mech 2011;165:212–8.
[53] Spitael P, Macosko CW. Strain hardening in polypropylenes and its role in extrusion foaming. Polym Eng Sci 2004;44:2090–100.
[54] Münstedt H, Steffl HT, Malmberg A. Correlation between rheological behavior in uniaxial elongation and film blowing properties of various polyethylenes. Rheol Acta 2005;45:14–22.
[55] Stange J, Münstedt H. Rheological properties and foaming behavior of polypropylenes with different molecular structure. J Rheol 2006;50:907–23.
[56] Kurzbeck S, Oster F, Münstedt H, Nguyen TQ, Gensler R. Rheological properties of two polypropylenes with different molecular structure. J Rheol 1999;43:359–74.
[57] Vinogradov GV, Fikhman VD, Radushkevich BV, Malkin AYa. Viscoelastic and relaxation properties of polystyrene melt on axial extension. J Polym Sci Part A-2 Polym Phys 1970;8:657–78.
[58] Kurbanaliev MK, Malkin AYa, Vinogradov GV. About growth of viscosity in pre-stationary deformation stage uniaxial stretching of polymers. Vysokomol Soedin B 1982;24:596–8 [in Russian].
[59] Rasmussen HK, Nielsen JK, Bach A, Hassager O. Viscosity overshoot in the start-up of uniaxial elongation of low density polyethylene melts. J Rheol 2005;49:369–81.
[60] McKinley GH, Hassager O. The Considère condition and rapid stretching of linear and branched polymer melts. J Rheol 1999;43:1195–212.
[61] Hassager O, Kolte VI, Renardy M. Failure and nonfailure of fluid filament in extension. J Non Newton Fluid Mech 1998;76:137–51.
[62] Petrie CJS. Considère reconsider: necking of polymer liquids. Chem Eng Sci 2009;64:4693–700.
[63] Barroso VS, Andrade BJ, Maia JM. An experimental study on the criterion for failure of polymer melts in uniaxial extension: the test case of a polyisobutylene melt in different deformation regimes. J Rheol 2011;54:605–18.
[64] Lentzakis H, Vlassopoulos D, Read DJ, Lee H, Chang T, Driva P, Hadjichristidis N. Uniaxial extensional rheology of well-characterized comby polymers. J Rheol 2013;57:605–25.
[65] Burghelea TI, Stary Z, Münstedt H. On the "viscosity overshoot" during the uniaxial extension of a low density polyethylene. J Non Newton Fluid Mech 2011;188:1198–209.
[66] Wagner MH, Rolón-Garrido VH. Constant force elongational flow of polymer melts: experiment and modeling. J Rheol 2012;56:1279–97.
[67] Alvarez NJ, Román JM, Huang ML, Michelsen ML, Hassager O. Creep measurements confirm steady flow after stress maximum in extension of branched polymer melts. Phys Rev Lett 2013;110, 168301/1–4.
[68] Stadler FJ, Kaschta J, Münstedt H, Becker F, Buback M. Influence of molecular mass distribution and long-chain branching on strain hardening of low density polyethylene. Rheol Acta 2009;48:478–90.
[69] Meissner J. Basic parameters, melt rheology, processing and end-use properties of three similar low density polyethylene samples. Pure Appl Chem 1975;42:553–612.
[70] Laun HM, Münstedt H. Comparison of elongational behavior of a polyethylene melt at constant stress and constant strain rate. Rheol Acta 1976;15:517–24.

[71] Laun HM, Münstedt H. Elongationalbehavior of a low-density polyethylene melt. 1. Strain rate and stress dependence of viscosity and recoverable strain in steady-state – comparison with shear data – influence of interfacial-tension. Rheol Acta 1978;17:415–25.
[72] Takahashi T, Takimoto JI, Koyama K. Uniaxial elongational viscosity of various molten polymer composites. Polym Compos 1999;20:357–66.
[73] van Ruymbeke E, Muliawan EB, Hatzikiriakos SG, Watanabe T, Hirao A, Vlassopoulos D. Viscoelasticity and extensional rheology of model Cayley-tree polymers of different generations. J Rheol 2010;54:643–62.
[74] Wagner MH, Raible T, Meissner J. Tensile stress overshoot in uniaxial extension of a LDPE melt. Rheol Acta 1979;18:427–8.
[75] Wagner MH, Bastian H, Hachmann P, Meissner J, Kurzbeck S, Münstedt H, Langouche F. The strain hardening behaviour of linear and long-chain-branched polyolefin melts in extensional flows. Rheol Acta 2000;39:97–109.
[76] Münstedt H, Kurzbeck S, Egerstdörger L. Influence of molecular structure on rheological properties of polyethylenes. Part II. Elongational behavior. Rheol Acta 1998;37:21–9.
[77] McLeish TCB, Larson RG. Molecular constitutive equations for a class of branched polymers: the pom-pom model. J Rheol 1998;42:81–110.
[78] McLeish TCB, Allgaier J, Bick DK, Bishko G, Biswas P, Blackwell R, Blottière B, Clarke N, Gibbs B, Groves DJ, Hakiki A, Heenan RK, Johnson JM, Kant R, Read R, Young N. Dynamics of entangled h-polymers: theory, rheology, and neutron-scattering. Macromolecules 1999;32:6734–58.
[79] Münstedt H. Dependence of the elongational behavior of polystyrene melts on molecular-weight and molecular-weight distribution. J Rheol 1980;24:847–67.
[80] Minegishi A, Nishioka A, Takahashi T, Masubuchi Y, Takimoto J, Koyama K. Uniaxial elongational viscosity of PS/a small amount of UHMW-PS blends. Rheol Acta 2001;40:329–38.
[81] Ye X, Larson RG, Pattamaprom C, Sridhar T. Extensional properties of monodisperse and bidisperse polystyrene solutions. J Rheol 2003;47:443–68.
[82] Wagner MH, Kheirandish A, Yamagichi M. Quantitative analysis of meltelongational behavior of LLDPE/LDPE melts. Rheol Acta 2004;44:198–218.
[83] Wagner MH, Kheirandish S, Koyama K, Nishioka A, Minegishi A, Takahashi T. Modeling strain hardening of polydisperse polystyrene melts by molecular stress electrospinning of linear homopolymers of poly(methyl methacrylate): exploring relationships between fiber formation, viscosity, function theory. Rheol Acta 2005;44:235–43.
[84] Wagner MH, Rubio P, Bastian H. The molecular structure function model for polydisperse polymer melts with dissipative convective constraint release. J Rheol 2001;45:1387–412.
[85] Wagner MH, Yamaguchi M, Takahashi M. Quantitative assessment of strain hardening of low-density polyethylene melts by the molecular stress function model. J Rheol 2003;47:779–93.
[86] Rolón-Garrido VH, Resch JA, Wolff F, Kaschta J, Münstedt H, Wagner MH. Prediction of the steady-state viscous and elastic properties of polyolefin melts in shear and elongation. Rheol Acta 2011;50:645–53.
[87] Malkin AYa. Non-Newtonian viscosity in steady-state shear flows. J Non Newton Fluid Mech 2013;192:48–65.
[88] Liu G, Sun H, Rangou S, Ntetsikas K, Avgeropoulos A, Wang SQ. Studying the origin of "strain hardening": basic difference between extension and shear. J Rheol 2013;57:89–104.
[89] Bhat PP, Appathurai S, Harris MT, Pasquali M, McKinley GH, Basaran OA. Formation of beads-on-a-string structures during breakup of viscoelastic filaments. Nat Phys 2010;6:625–31.
[90] Ardecani AM, Sharma V, McKinley GH. Dynamics of bead formation, filament thinning and breakup in weakly viscoelastic jets. J Fluid Mech 2010;665:46–56.
[91] McKinley GH. Dimensionless groups for understanding free surface flows of complex fluids. Soc Rheol Bull 2005;74:6–10.
[92] Ohnesorge W. Formation of drops by nozzles and the breakup of liquid jets. J Appl Math Mech 1936;16:355–8.
[93] Kulichikhin VG, Malkin AYa, Semakov AV, Skvostsov IYu, Arinstein A. Jet instability due to stretch-induced phase separation in polymer solutions. Eur Phys J E 2014;37:10.
[94] Gier S, Wagner C. Visualization of the flow profile inside a thinning filament during capillary breakup of a polymer solution via particle image velocimetry and particle tracking velocimetry. Phys Fluids 2012;24, 053102/1–13.
[95] Greenfeld I, Fezzaa K, Rafailovich MH, Zussman E. Fast X-ray phase-contrast imaging of electrospinning polymer jets: measurements of radius, velocity, and concentration. Macromolecules 2012;45:3616–26.
[96] Hassager O, Morgensten K, Bach A, Almdal K, Rasmussen HK, Pyckhout-Hintzen W. Stress and neutron scattering measurements on linear polymer melts undergoing steady elongational flow. Rheol Acta 2012;51:385–94.
[97] Krőger R, Berg S, Delgado A, Rath HJ. Stretching behaviour of large polymeric and Newtonian liquid bridges in plateau simulation. J Non Newton Fluid Mech 1992;45:385–400.
[98] Berg S, Krőger R, Rath HJ. Measurement of extensional viscosity by stretching large liquid bridges in microgravity. J Non Newton Fluid Mech 1994;55:307–19.
[99] Gaudet S, McKinley GH, Stone HA. Extensional deformation of Newtonian liquid bridges. Phys Fluids 1996;8:2568–79.
[100] Castrejón-Pita AA, Castrejón-Pita J, Hutchings IM. Breakup of liquid filaments. Phys Rev Lett 2012;108, 074506/1–4.
[101] Middleman S. Stability of a viscoelastic jet. Chem Eng Sci 1965;20:1037–40.
[102] Goldin M, Yerushalmi J, Pfeffer R, Shinnar R. Breakup of a laminar capillary jet of a viscoelastic fluid. J Fluid Mech 1969;38:689–711.
[103] Li J, Fontelos MA. Drop dynamics on the beads-on-string structure of viscoelastic jets: a numerical study. Phys Fluids 2003;15:922–37.
[104] Oliveira MSN, McKinley GH. Iterated stretching and multiple beads-on-a-string phenomena in dilute solutions of high extensible flexible polymers. Phys Fluids 2005;17, 0171704/1–4.
[105] Wagner C, Amarouchene Y, Bonn D, Eggers J. Droplet detachment and satellite bead formation in viscoelastic fluids. Phys Rev Lett 2005;95, 64504/1–4.
[106] Clasen C, Eggers J, Fontelos MA, Li J, McKinley GH. The beads-on-string structure of visco-elastic jets. J Fluid Mech 2006;556:283–308.
[107] Sostarcez MC, Belmonte A. Beads-on-string phenomena in worm-like micellar fluids. Phys Fluids 2004;16:L67–70.
[108] Sridhar T, Tirtaatmadja V, Nguyen DA, Gupta RK. Measurement of extensional viscosity of polymer solutions. J Non Newton Fluid Mech 1991;40:271–80.
[109] Spiegelberg SH, Ables DC, McKinley GH. The role of end-effects on measurements of extensional viscosity in filament stretching rheometers. J Non Newton Fluid Mech 1996;64:229–67.
[110] Solomon MJ, Muller SJ. The transient extensional behavior of polystyrene-based Boger fluids of varying solvent quality and molecular weight. J Rheol 1996;40:837–56.
[111] Spiegelberg SH, McKinley GH. Stress relaxation and elastic decohesion of viscoelastic polymer solutions in extensional flow. J Non Newton Fluid Mech 1996;67:49–76.
[112] Yao M, McKinley GH. Numerical simulation of extensional deformations of viscoelastic liquid bridges in filament stretching devices. J Non Newton Fluid Mech 1998;74:47–88.
[113] Oldroyd JG. On the formulation of rheological equations of state. Proc Roy Soc A 1950;200:523–41.
[114] Fontelos MA, Li J. On the evolution and rupture of filaments in Giesekus and FENE models. J Non Newton Fluid Mech 2004;118:1–16.
[115] Renardy M, Losh D. Similarity solutions for jet breakup in a Giesekus fluid with inertia. J Non Newton Fluid Mech 2002;106:17–27.
[116] Renardy M. A numerical study of the asymptotic evolution and breakup of Newtonian and viscoelastic jets. J Non Newton Fluid Mech 1995;59:262–7.
[117] Bousfield DW, Keunings R, Marrucci G, Denn MM. Nonlinear analysis of the surface-tension driven breakup of viscoelastic fluid filaments. J Non Newton Fluid Mech 1986;21:79–97.
[118] Malkin AYa, Kulichikhin SG, Chalykh AE. The effect of deformation on the phase separation of the polycaproamide–caprolactam system. Polymer 1981;22:1373–6.
[119] Larson RG. Flow-induced mixing, demixing, and phase transitions in polymeric fluids. Rheol Acta 1992;31:497–520.
[120] Peterlin A. Crystallization from a strained melt or solution. Polym Eng Sci 1976;16:126–35.
[121] Rangel-Nafaile C, Metzner AB, Wissbrun RF. Analysis of stress-induced phase separations in polymer solutions. Macromolecules 1984;17:1187–95.
[122] Janeschitz-Kriegl H, Ratajski E, Stadbauer M. Flow as an effective promotor of nucleation in polymer melts: a quantitative evaluation. Rheol Acta 2003;42:355–64.
[123] Stadbauer M, Janeschitz-Kriegl H, Eder G, Ratajski E. New extensional rheometer for creep flow at high tensile stress. Part II.

Flow induced nucleation for the crystallization of iPP. J Rheol 2004;48:631–9.
[124] Holmqvist P, Lettinga MP, Buitenhuis J, Dhont JKG. Crystallization kinetics of colloidal spheres under stationary shear flow. Langmuir 2005;21:10976–82.
[125] Hadinata S, Boos D, Gabriel C, Wassner E, Rüllmann M, Kao N, Laun HM. Elongation-induced crystallization of a high molecular weight polybutene-1 melt compared to shear-induced crystallization. J Rheol 2007;51:195–215.
[126] White EEB, Winter HH, Rothstein JB. Extensional-flow-induced crystallization. Rheol Acta 2012;51:303–14.
[127] Derakhshandeh M, Hatzikiriakos SG. Flow induced crystallization of high-density polyethylene: the effect of shear and uniaxial extension. Rheol Acta 2012;51:315–27.
[128] Frenkel' SYa, Baranov VG, Bel'nikevich NG, Panov YuN. Orientation mechanism of solid phase formation in polymer solutions subjected to a longitudinal hydrodynamic field. Polym Sci USSR 1964;6:2124–5 [Vysokomol Soedin 1964; 6:1917–8].
[129] Frenkel' SYa, Agranova AS, Aldoshin VG, Baranov VG, Korzhavin LN, Panov YuN, Samsonova TI. On orientation mechanism of the solid phase formation in moderately concentrated polymer solutions (direct observation of longitudinal flow). Ukr Phys J 1967;12:282–9.
[130] Sattler S, Wagner C, Eggers J. Blistering pattern and formation of nanofibers in capillary thinning of polymer solutions. Phys Rev Lett 2008;100, 164502/1–4.
[131] Sattler R, Gier S, Eggers J, Wagner C. The final stages of capillary break-up of polymer solutions. Phys Fluids 2012;24, 023101/1–2.
[132] Kapitsa PL. Wave flow of thin layers of a viscous liquid. I. Free flow. J Exp Theor Phys 1948;18:3–19.
[133] Levich VG. Physico-chemical hydrodynamics. Englewood Cliffs, NJ: Prentice Hall; 1962, 700 pp.
[134] Yarin AL, Oron A, Rosenau Ph. Capillary in stability of thin liquid film on a cylinder. Phys Fluids A 1993;5, 91/1–8.
[135] Oron A, Davis SH, Bankoff SG. Long-scale evolution of thin liquid films. Rev Mod Phys 1997;69:931–80.
[136] Johnson M, Kamm RD, Hoi LW, Shapiro A, Pedley TJ. The nonlinear growth of surface-tension-driven instabilities of a thin annular film. J Fluid Mech 1991;233:141–56.
[137] Gilet T, Terwagne D, Vandewalle N. Droplets sliding on fibres. Eur Phys J E 2010;31:253–62.
[138] Taylor GI. Disintegration of water drops in an electric field. Proc R Soc A 1964;280:383–97.
[139] Taylor GI. The circulation produced in a drop by an electric field. Proc R Soc A 1966;291:159–66.
[140] Taylor GI. Electrically driven jets. Proc R Soc A 1969;313:453–75.
[141] Spivak AF, Dzenis YA, Reneker DH. A model of steady state jet in the electrospinning process. Mech Res Commun 2000;27:37–42.
[142] Arinstein A, Zussman E. Electrospun polymer nanofibers: mechanical and thermodynamic perspectives. J Polym Sci B Polym Phys 2011;49:691–707.
[143] Chang HC, Demekhin EA, Kalaidin E. Iterated stretching of viscoelastic jets Iterated stretching of viscoelastic jets. Phys Fluids 1999;11:1717–37.
[144] Huang ZhM, Zhang YZ, Kotaki M, Ramakrishna S. A review on polymer nanofibers by electrospinning and their applications in nanocomposites. Compos Sci Technol 2003;63:2223–53.
[145] Li D, Xia Y. Electrospinning of nanofibers: reinventing the wheel. Adv Mater 2004;16:1151–70.
[146] Reneker DH, Yarin AL, Zussman E, Xu H. Electrospinning of nanofibers from polymer solutions and melts. Adv Appl Mech 2007;41:43–195.
[147] Reneker DH, Yarin AL. Electrospinning jets and polymer nanofibers. Polymer 2008;49:2387–425.
[148] Yoshioka T, Dersch R, Greiner A, Tsuji M, Schaper AK. Highly oriented crystalline PE nanofibrils produced by electric-field-induced stretching of electrospun wet fibers. Macromol Mater Eng 2010;295:1082–9.
[149] Reznik SN, Zussman E. Capillary-dominated electrified jets of a viscous leaky dielectric liquid. Phys Rev E 2009;81, 026313/1–7.
[150] Han T, Yarin AL, Reneker DG. Viscoelastic electrospun jets: initial stresses and elongational rheometry. Polymer 2008;49:1651–8.
[151] Bellan LM, Craighead HG, Hinestroza JP. Direct measurement of fluid velocity in an electrospinning jet using particle image velocimetry. J Appl Phys 2007;102, 094308/1–5.
[152] Koombhongse S, Liu W, Reneker DH. Flat polymer ribbons and other shapes by electrospinning. J Polym Sci B Polym Phys 2001;39:2598–606.
[153] Bognitzki M, Czado W, Frese T, Schaper A, Hellwig M, Steinhart M, Greiner A, Wendorff JH. Nanostructured fibers via electrospinning. Adv Mater 2001;13:70–2.
[154] Wu XF, Salkovskiy Yu, Dzenisc YuA. Modeling of solvent evaporation from polymer jets in electrospinning. Appl Phys Lett 2011;98, 223108/1–3.
[155] Tripatanasuwan S, Zhong ZX, Reneker DH. Effect of evaporation and solidification of the charged jet in electrospinning of poly(ethylene oxide) aqueous solution. Polymer 2007;48:5742–6.
[156] Wang C, Cheng YW, Hsu CH, Chien HC, Tsou SY. How to manipulate the electrospinning jet with controlled properties to obtain uniform fibers with the smallest diameter? A brief discussion of solution electrospinning process. J Polym Res 2011;18:111–23.
[157] Zussman E, Rittel D, Yarin AL. Failure modes of electrospun nanofibers. Appl Phys Lett 2003;82:3958–60.
[158] Burton EF, Wiegand WB. Effect of electricity on streams of water drops. Philos Mag 1912;23:148–65.
[159] Zeleny J. The electrical discharge from liquid points, and a hydrostatic method of measuring the electric intensity at their surfaces. Phys Rev 1914;3:69–91.
[160] Zeleny J. On the conditions of instability of electrified drops, with applications to the electrical discharge from liquid points. Proc Camb Philos Soc 1915;18:71–83.
[161] Zeleny J. Instability of electrified liquid surfaces. Phys Rev 1917;10:1–6.
[162] Zeleny J. Electrical discharges from pointed conductors. Phys Rev 1920;16:102–25.
[163] Macky WA. Some investigations on the deformation and breaking of water drops in strong electric fields. Proc R Soc A 1931;133:565–87.
[164] Reneker DH, Yarin AL, Fong H, Koombhongse S. Bending instability of electrically charged liquid jets of polymer solutions in electrospinning. J Appl Phys 2000;87:4531–47.
[165] Yarin AL, Koombhongse S, Reneker DH. Bending instability in electrospinning of nanofibers. J Appl Phys 2001;89:3018–26.
[166] Hohman MM, Shin M, Rutledge G, Brenner MP. Electrospinning and electrically forced jets. I. Stability theory. Phys Fluids 2001;13:2201–20.
[167] Shin YM, Hohman MM, Brenner MP, Rutledge GC. Electrospinning: a whipping fluid jet generates submicron polymer fibers. Appl Phys Lett 2001;78:1149–51.
[168] Bellan LM, Craighead HG. Molecular orientation in individual electrospun nanofibers measured via polarized Raman spectroscopy. Polymer 2008;49:3125–9.
[169] Richard-Lacroix M, Pellerin C, Orientation. Structure of single electrospun nanofibers of poly(ethylene terephthalate) by confocal Raman spectroscopy. Macromolecules 2012;45:1946–53.
[170] Yoshioka T, Dersch R, Greiner A, Tsuji M, Schaper AK. Orientation analysis of individual electrospun PE nanofibers by transmission electron microscopy. Polymer 2010;51:2383–9.
[171] Kolbuk D, Sajkiewicz P, Kowalewski TA. Optical birefringence and molecular orientation of electrospun polycaprolactone fibers by polarizing-interference microscopy. Eur Polym J 2012;48:275–83.
[172] Higuera FJ. Stationary viscosity-dominated electrified polymer jets. J Fluid Mech 2006;558:143–52.
[173] Subbotin AV. Scaling analysis of a charges jet formed at electrospinning of a viscoelastic fluid. Colloid J 2012;74:530–4.
[174] Theron SA, Zussman E, Yarin AL. Experimental investigation of the governing parameters in the electrospinning of polymer solutions. Polymer 2004;45:2017–30.
[175] Yu JH, Fridrikh SV, Rutledge GC. The role of elasticity in the formation of electrospun fibers. Polymer 2006;47:4789–97.
[176] Larrondo L, Manley RSJ. Electrostatic deformation of a pendant drop of polymer melt. J Polym Sci B Polym Phys 1981;19:909–20.
[177] Greenfeld I, Arinstein A, Fezzaa K, Rafailovich MH, Zussman E. Evolution of polymer solution structure during electrospinning: simplest theoretical model and experimental observations. Phys Rev E 2011;84, 041806/1–9.
[178] Gupta P, Elkins C, Long TE, Wilkes GL. Electrospinning of linear homopolymers of poly(methyl methacrylate): exploring relationships between fiber formation, viscosity, molecular weight and concentration in a good solvent. Polymer 2005;46:4799–810.
[179] deGennes PG. Coil-stretch transition of dilute flexible polymers under ultrahigh velocity gradients. J Chem Phys 1974;60:5030–42.
[180] Balabaev NK, Borodin IP, Borodina TI, Khazanovich TN. Stretching of a semiflexible chain composed of elastic bonds. Polym Sci A 2010;52:655–61 [Vysokomol Soedin A 2010;52:993–9].
[181] Treloar LRG. The physics of rubberlike elasticity. 3rd ed. Oxford, UK: Clarendon; 1975, 370 pp.

[182] Gent AN. Rubber elasticity: basic concepts and behavior. In: Mark JE, Burak E, editors. Science and technology of rubber. 3rd ed. Amsterdam: Elsevier; 2005. p. 1–27.
[183] Edwards SF. The statistical mechanics of polymerized material. Proc Phys Soc 1967;92:9–16.
[184] Doi N, Edwards SF. The theory of polymer dynamics. Oxford, UK: Oxford University Press; 1986, 416 pp.
[185] Colby RH, Rubinstein M. Two-parameter scaling for polymers in Θ solvents. Macromolecules 1990;23:2753–7.
[186] Graham RS, Likhman AE, McLeish TCB, Milner ST. Microscopic theory of linear, entangled polymer chains under rapid deformation including chain stretch and convective constraint release. J Rheol 2003;47:1171–200.
[187] Milner ST. Predicting the tube diameter in melts and solutions. Macromolecules 2005;38:4929–39.
[188] McLeish TCB. Tube theory of entangled polymer dynamics. Adv Phys 2002;51:1379–527.
[189] McLeish T. Molecular polymeric matter, Weissenberg, Astbury and the pleasure of being wrong. Rheol Acta 2008;47:479–89.
[190] Read DJ. Convective constraint release with chain stretch: solution of the Rouse-tube model in the limit of infinite tubes. J Rheol 2004;48:349–77.
[191] Qin J, Milner ST. Tube diameter of oriented and stretched polymer melts. Macromolecules 2013;46:1659–72.
[192] Xu F, Denn MM, Scheiber JD. A full-chain stochastic tube model for entangled melts and solutions of linear polymers. J Rheol 2006;50:477–96.
[193] Park J, Mead DW, Denn MM. Stochastic simulation of entangled polymeric liquids in fast flows: microstructure modification. J Rheol 2012;56:1057–81.
[194] Giesekus H. A simple constitutive equation for polymer fluids based on the concept of deformation-dependent tensorial mobility. J Non Newton Fluid Mech 1982;11:69–109.